International Journal of Nanomedicine

Dovepress
open access to scientific and medical research

Open Access Full Text Article

ORIGINAL RESEARCH

GO/Cu Nanosheet-Integrated Hydrogel Platform as a Bioactive and Biocompatible Scaffold for Enhanced Calvarial Bone Regeneration

Ying Yang[1–3,*], Bixia Zhou[1,2,*], Min Li[4], Yishuai Sun[1,2], Xulei Jiang[1,2], Xinxin Zhou[1,2], Chengjun Hu[1,2], Dou Zhang[3], Hang Luo[3], Wuyuan Tan[1,2], Xinghua Yang[1,2], Shaorong Lei[1,2]

[1]Department of Plastic Surgery, Xiangya Hospital, Central South University, Changsha, Hunan, People's Republic of China; [2]National Clinical Research Center for Geriatric Disorders, Xiangya Hospital Central South University, Changsha, Hunan, People's Republic of China; [3]State Key Laboratory of Powder Metallurgy, Central South University, Changsha, Hunan, People's Republic of China; [4]Department of Oncology, Changsha Central Hospital, University of South China, Changsha, Hunan, People's Republic of China

*These authors contributed equally to this work

Correspondence: Shaorong Lei, Department of Plastic Surgery, Xiangya Hospital, Central South University, 87 Xiangya Road, Changsha, Hunan, 410008, People's Republic of China, Tel +86 73189753014, Email leishaorong@csu.edu.cn; Xinghua Yang, Department of Plastic Surgery, Xiangya Hospital, Central South University, 87 Xiangya Road, Changsha, Hunan, 410008, People's Republic of China, Tel +86 73189753014, Email yxhua8805@sina.com

Purpose: The treatment of craniofacial bone defects caused by trauma, tumors, and infectious and degenerative diseases is a significant issue in current clinical practice. Following the rapid development of bone tissue engineering (BTE) in the last decade, bioactive scaffolds coupled with multifunctional properties are in high demand with regard to effective therapy for bone defects. Herein, an innovative bone scaffold consisting of GO/Cu nanoderivatives and GelMA-based organic-inorganic hybrids was reported for repairing full-thickness calvarial bone defect.

Methods: In this study, motivated by the versatile biological functions of nanomaterials and synthetic hydrogels, copper nanoparticle (CuNP)-decorated graphene oxide (GO) nanosheets (GO/Cu) were combined with methacrylated gelatin (GelMA)-based organic-inorganic hybrids to construct porous bone scaffolds that mimic the extracellular matrix (ECM) of bone tissues by photocrosslinking. The material characterizations, in vitro cytocompatibility, macrophage polarization and osteogenesis of the biohybrid hydrogel scaffolds were investigated, and two different animal models (BALB/c mice and SD rats) were established to further confirm the in vivo neovascularization, macrophage recruitment, biocompatibility, biosafety and bone regenerative potential.

Results: We found that GO/Cu-functionalized GelMA/β-TCP hydrogel scaffolds exhibited evidently promoted osteogenic activities, M2 type macrophage polarization, increased secretion of anti-inflammatory factors and excellent cytocompatibility, with favorable surface characteristics and sustainable release of Cu^{2+}. Additionally, improved neovascularization, macrophage recruitment and tissue integration were found in mice implanted with the bioactive hydrogels. More importantly, the observations of microCT reconstruction and histological analysis in a calvarial bone defect model in rats treated with GO/Cu-incorporated hydrogel scaffolds demonstrated significantly increased bone morphometric values and newly formed bone tissues, indicating accelerated bone healing.

Conclusion: Taken together, this BTE-based bone repair strategy provides a promising and feasible method for constructing multifunctional GO/Cu nanocomposite-incorporated biohybrid hydrogel scaffolds with facilitated osteogenesis, angiogenesis and immunoregulation in one system, with the optimization of material properties and biosafety, it thereby demonstrates great application potential for correcting craniofacial bone defects in future clinical scenarios.

Keywords: nanomaterials, hybrid hydrogel, bone scaffolds, craniofacial bone defects, bone regeneration

Introduction

Although enormous progress has been made in bone reconstruction in terms of clinical countermeasures and bone tissue engineering, efficiently repairing craniofacial bone defects resulting from severe trauma, tumors, and infectious and degenerative diseases is still a substantial challenge for plastic surgeons.[1–4] To achieve satisfactory therapeutic outcomes, autologous, allogenic

Received: 4 May 2024
Accepted: 7 August 2024
Published: 14 August 2024

Graphical Abstract

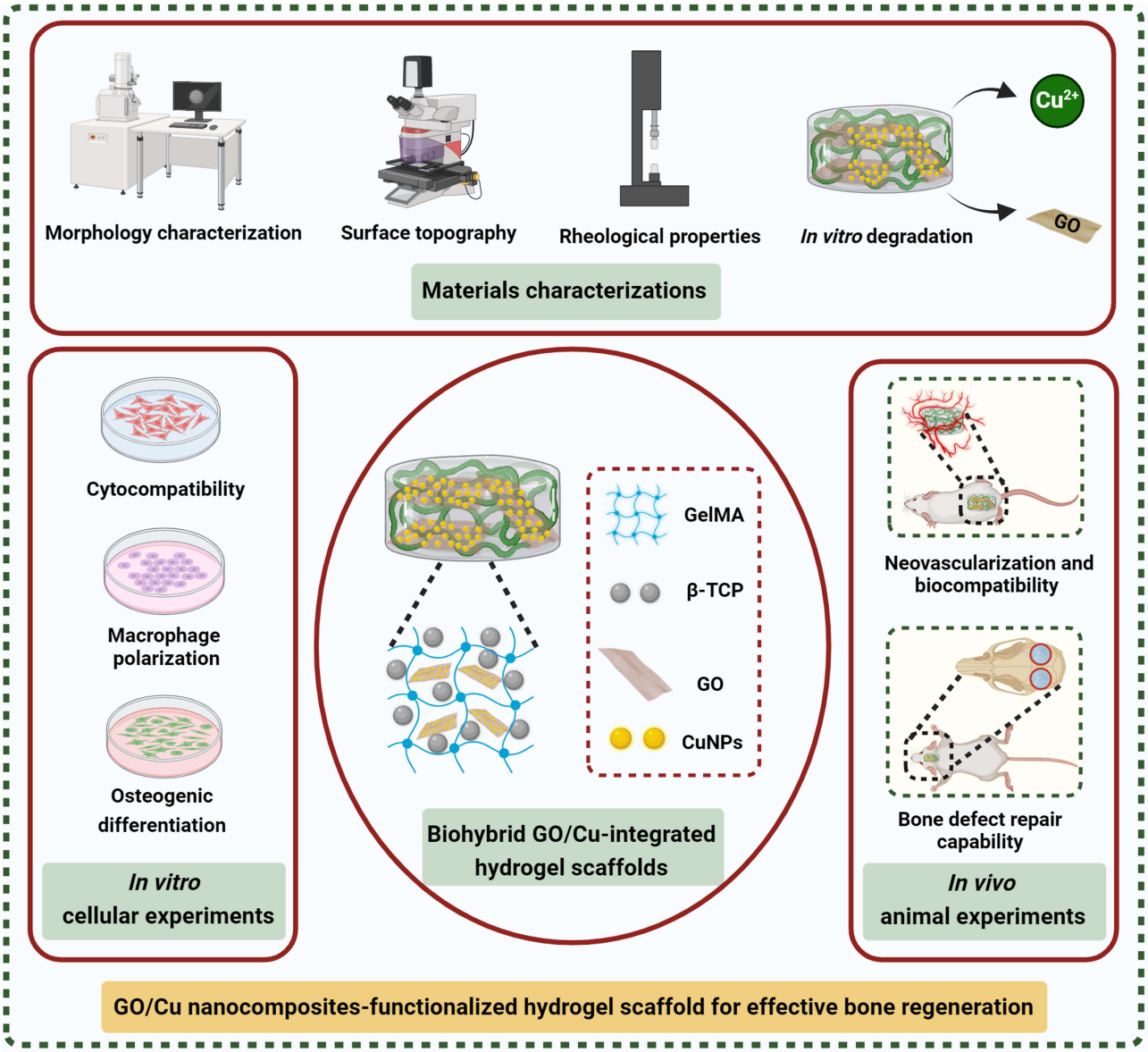

and artificial bone grafts have been extensively applied in current clinical scenarios.[5] Nevertheless, the clinical promotion and application of these grafts are always restricted due to donor site injury, limited availability, potential infectious disease transmission, immunological rejection and substantial economic burden.[5–7] As an alternative approach to satisfy the ever-increasing demand for bone repair, bone tissue engineering (BTE) has been a research hotspot for the last decade that has shown improvements in material science, processing techniques and in-depth understanding of bone healing mechanisms.[5,8,9] Specifically, angiogenesis and osteogenesis are two significant factors involved in the stable and sturdy remodeling processes for bone regeneration.[10] Considering the complexity of the bone repair microenvironment and functional diversity deficiency of current bone repair substitutes, developing an innovative restoration system with multifunctions (osteogenesis, angiogenesis and immunoregulation) for more effective treatment of craniofacial bone defects is particularly urgent, but also challenging.

It has been confirmed that a series of complicated and well-organized biological events (inflammation, maturation and remodeling) occur during the process of bone repair.[10,11] Undoubtedly, BTE-based bone repair strategies provide visible and efficient therapeutic outcomes for the growing incidence of bone fractures or defects, and the principal function of the implanted

biomaterials designated for bone regeneration is to serve as a temporary local niche that provides a favorable microenvironment for cell (immune, vascular endothelial and mesenchymal stem cells) recruitment, adherence, proliferation and differentiation.[11] In addition, macrophages play a critical role in bone healing due to their various functions in multiple aspects of bone repair, including inflammatory regulation, angiogenesis and stimulation of cell differentiation, which are closely related to bone tissue formation.[11] Considering the significance of macrophage behavior in bone tissue healing, scaffolds with immunomodulatory properties were designated to improve the inflammatory microenvironment and accelerate bone defect reconstruction.[12,13] Therefore, biomimetic scaffolds coupled with osteogenesis, angiogenesis and immunoregulation could be promising candidates for improving bone repair and regeneration.

The extracellular matrix (ECM) is a significant component of bone tissues and is also fundamental in mineralization and bone maturation. Notably, the structural capacity and effective interaction with the ECM should be taken into consideration when biomimetic scaffolds are used for BTE applications.[8] Gelatin-based hydrogels exhibit great application prospects in tissue therapeutics due to their hydrated polymeric networks that mimic the biological ECM.[7] Among these gelatin-based hydrogels, methacrylated gelatin (GelMA) is an ideal physicochemical mimetic of the natural ECM due to its excellent biodegradability, biocompatibility and tunable physical characteristics.[14,15] Currently, GelMA-based biomaterials have been extensively studied for their various biological applications ranging from drug delivery to tissue engineering; however, the poor osteogenic properties of pure GelMA hydrogels restrict their application in BTE.[15] Thus, multiple strategies have been devoted to promoting the osteoinductivity and osteoconductivity of GelMA hydrogels through the incorporation of nanomaterials, inorganic ingredients, bioactive molecules or metallic ions, making GelMA hydrogels more suitable for correcting bone damage.[3,4,16–19] Graphene and its derivatives (GO or rGO) have demonstrated promising application potential in tissue regeneration, nanocatalysis and biomedical fields due to their versatile characteristics, such as good electrical and mechanical conductivity properties and high capacity for heat isolation and absorption.[20] Moreover, the introduction of GO could improve the mechanical properties and biological activities of hybrid scaffolds, significantly promoting cell attachment, migration, proliferation and differentiation of osteoblasts.[21] During continuous innovation and modification in material processing, surface characterization, and optimization of the bioactivity and cytotoxicity of GO in recent years, GO-based biomaterials have shown unique advantages with regard to constructing BTE scaffolds for repairing bone defects.[21–23] Specifically, the improvement of osteogenic actions of GO nanosheets may be closely related to the positive effects on cell–cell or cell–material interactions, leading to increased expression of osteogenesis-associated genes via activating MAPK, JNK and FoxO1 signal pathways.[22] However, the promotive efficacy and biosafety of GO-incorporated bone scaffolds needs to be further investigated and elucidated prior to popularization in future clinical settings.

The rapid development of metal ion-modified composite scaffolds in BTE applications displayed satisfactory therapeutic effects in bone repair under specific conditions, attributing to their versatility in stimulating osteogenesis and angiogenesis and preventing bacterial infection and osteoclast activity.[24] In our previous works, copper nanoparticle (CuNP)-decorated GO nanosheets (GO/Cu) were successfully manufactured, and the antibacterial activities, cytocompatibility and therapeutic effects on bacteria-infected wound defects were explored and confirmed.[25,26] With the arduous efforts and initial achievements in GO-based nanocomposite functionalization of our team, and determined osteogenic and angiogenic activities of copper ions, herein, an innovative bone scaffold consisting of GO/Cu nanoderivatives and GelMA-based organic-inorganic hybrids was reported, and its material characterizations, in vitro cytocompatibility, macrophage polarization and osteogenic properties were systematically studied, followed by the establishment of different animal models in mice and rats to further clarify its in vivo neovascularization, macrophage recruitment, biocompatibility, biosafety and bone healing capabilities (Scheme 1). It is anticipated that the combination of GO/Cu nanocomposites and β-TCP-incorporated GelMA hydrogels could enrich the biofunctions of biomimetic scaffolds with no observed physiological detriments, providing new insights into the construction of regenerative implants for bone defects and bone regeneration.

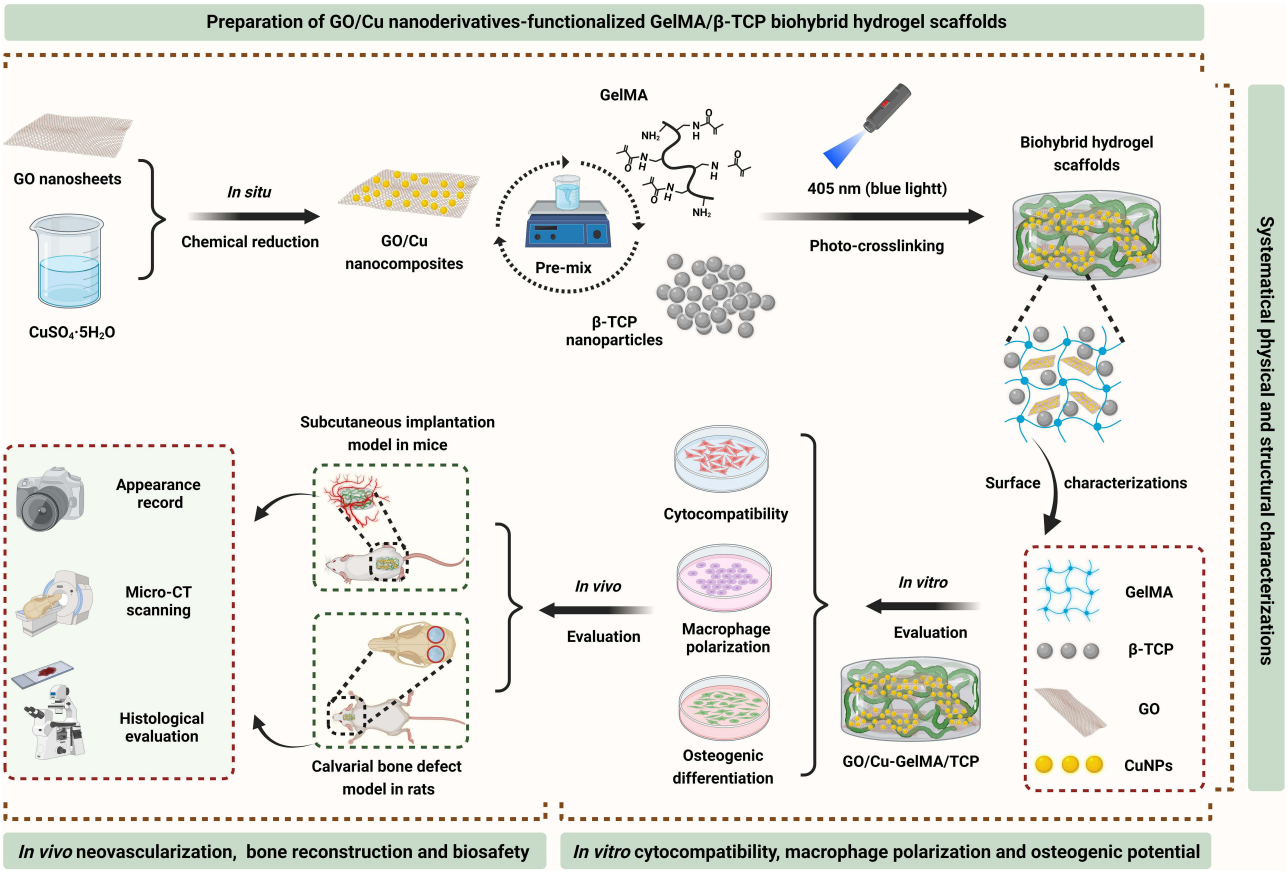

Scheme 1 Schematic description of the concept of integrating GO/Cu nanocomposites into β-TCP-incorporated GelMA hydrogel to promote calvarial defect restoration (created with BioRender.com).
Abbreviations: β-TCP, beta tricalcium phosphate; GelMA, methacrylated gelatin; GO/Cu, copper nanoparticle-decorated graphene oxide nanosheets.

Materials and Methods

Preparation of GO/Cu Nanosheets and GO/Cu-Functionalized GelMA/β-TCP Hydrogel Scaffold

GO/Cu nanosheets were synthesized by an in situ chemical reduction method, according to our previous works, before the fabrication of biohybrid hydrogel scaffolds.[25,26] Briefly, the as-prepared GO nanosheet suspension (Aladdin, Shanghai, China) was mixed and agitated adequately with desired amounts of $CuSO_4.5H_2O$ and EDTA ($2Na.2H_2O$) for approximately 1 h at 30 °C, followed by the addition of chemical reduction solutions (NaOH and $NaBH_4$) and agitation for 30 min. Then, uniform GO/Cu nanosheets with a mass ratio of 2:1 were obtained after washing, centrifugation and drying sequentially. Subsequently, a photocrosslinking procedure was used to prepare GO/Cu nanosheet-integrated hydrogel scaffolds.[17,27] Briefly, 5 mg of lithium phenyl-2,4,6-trimethyl-benzoylphosphinate (LAP, EFL, Suzhou, China) was dissolved in 20 mL of phosphate buffer solution (PBS) for 20 min at 45 °C in a water bath (DXY-1T, Dingxinyi Experimental Equipment Co., Ltd., Shenzhen, China) away from light to serve as a photoinitiator (0.25% w/v). Then, 1 g of lyophilized GelMA with 60% substitution (GM60, EFL) was added to 20 mL of LAP solution and dissolved thoroughly at 65 °C for 30 min to obtain a homogeneous prepolymer solution (5% w/v), followed by aseptic filtration through 0.22 μm sterile filters (Millipore, Merck, Darmstadt, Germany) and storage in a water bath at 37 °C to avoid gelation. Finally, the desired amounts of beta tricalcium phosphate (β-TCP, Macklin Biochemical Co., Ltd., Shanghai, China) nanoparticles (10% wt, 100 mg) and GO/Cu nanosheets (2.0% wt, 20 mg) were added into the GelMA solution to obtain GO/Cu-integrated GelMA/TCP hybrid hydrogel scaffolds (G/T/GO/Cu) after being exposed to blue light (405 nm, 3 W, EFL-LS-1600-405) for approximately 20 to 30s at room temperature. Similarly, GelMA (G), GelMA/TCP (G/T), and GO nanosheet-incorporated GelMA/TCP (G/T/GO) hydrogel scaffolds were also prepared and served as controls.

Physical and Structural Characterizations

To observe the gelation process of the hydrogel scaffolds directly, digital photographs were recorded and compared. Then, the microstructures of the hydrogel scaffolds were observed by a field-emission scanning electron microscope (FE-SEM, TESCAN MIRA LMS, Brno-Kohoutovice, Czech Republic) with an accelerating voltage of 10 kV. The elemental distribution (C, O, N, P, Ca and Cu) of the hybrid hydrogel scaffolds was examined and recorded by energy-dispersive X-ray spectroscopy (EDS, Xplore, TESCAN). Three-dimensional laser microscopy (KEYENCE VK-X150, Olympus Corporation, Tokyo, Japan) was applied to detect the surface topography of the biohybrid hydrogel scaffolds, followed by acquisition of 3D laser scanning images and quantitative analysis of the surface roughness. The rheological properties of the hydrogel scaffolds were confirmed by a Discovery HR2 Hybrid Rheometer (TA Instruments, Waters Corporation, USA). Hydrogel scaffolds with a diameter of 20 mm were prepared using a Peltier plate geometry, and oscillatory strain sweep (0.01% to 100% strain, 1 Hz frequency) measurements were performed to examine the linear viscoelastic response at 25 °C. Meanwhile, frequency sweep measurements (0.1 to 100 Hz, 0.5% strain) were also performed and recorded. The static water contact angles (WCAs) of the hydrogel scaffolds were recorded and measured on a contact angle analyzer (LSA-100, LAUDA Scientific GmhH, Germany), and the volume of water droplets was approximately 20 μL. The interaction between GO/Cu nanosheets and GelMA polymers within the hydrogel network and relevant functional groups was confirmed by Fourier transform infrared spectroscopy (FT-IR, Nicolet iS20, Thermo Fisher Scientific, MA, USA) with a resolution of 4.0 cm^{-1} and 32 scans per scaffold ranging from 4000 to 400 cm^{-1}. X-ray photoelectron spectroscopy (XPS, K-Alpha, Thermo Fisher Scientific) was used to observe the distribution and valence state of elements grown over the hydrogel scaffolds. The excitation source of XPS was Al Kα with 1486.6 eV at a voltage of 12 kV and electricity of 6 mA. Moreover, a thermogravimetric analyzer (TGA, STA 449F3, Netzsch, Germany) was applied to investigate the thermal degradation behavior of the hydrogel scaffolds under nitrogen flow (20 mL/min), and the heating rate and range were 10 °C/min and 30 to 1100 °C, respectively. To determine the swelling behavior of the hydrogel scaffolds, prepared samples (diameter × thickness: 2 cm × 0.5 cm) were lyophilized and weighed to obtain the dry weight (Wd). Subsequently, dehydrated scaffolds were immersed in ddH_2O for 2, 24 and 48 h at 25 °C, and the swollen weight (Ws) of the scaffolds was recorded after removal of excess water on filter paper. The swelling ratio of each sample was expressed as (Ws − Wd)/Wd as previously described.[4]

In vitro Degradation Behavior of the Hydrogel Scaffold

The in vitro release kinetics of Cu^{2+} from the GO/Cu-integrated hydrogel scaffolds (diameter × thickness: 2.5 cm × 1.0 cm) were confirmed after being soaked in HEPES buffer (Sigma-Aldrich, MO, USA) with different pH values (5.5, 7.4 and 8.5) at 37 °C, and samples were incubated on a shaker at 100 rpm for up to 21 d.[26] The degradation liquids were collected and refreshed at each indicated time point (Days 0, 1, 3, 5, 7, 9, 11, 13, 15, 17, 19 and 21), and the obtained supernatant was then examined by using inductively coupled plasma-optical emission spectrometry (ICP-OES, Optima 5300 DV, PerkinElmer, USA) to further determine the amount of copper ions released from the hydrogel scaffolds at each time point. In addition, the in vitro biodegradability of the hydrogels was investigated by the weighting method with some modifications as previously reported.[28,29] Briefly, hydrogel scaffolds were immersed in 500 μL of collagenase type II (1.5 U/mL, 2275MG100, neoFroxx GmbH, Germany) PBS solution in a 12-well plate and incubated at room temperature for two weeks. The collagenase solution in each well was refreshed daily to maintain constant enzymatic activity. The hydrogels were weighed daily after removing the moisture over the surface of the hydrogels. The initial mass of hydrogels was considered as W_0, and the remaining mass was recorded as W_1 obtained at each time point. Therefore, the mass remaining ratio was calculated as the following: Remaining mass ratio (%) = $W_1/W_0 \times 100\%$.

In vitro Cytocompatibility and Macrophage Polarization

Preparation and Culture of Cells

Bone mesenchymal stem cells (BMSCs) were isolated from the bone marrow of male Sprague-Dawley (SD) rats as previously reported.[30,31] RAW264.7 cells were purchased from the Cell Bank of the Chinese Academy of Science (Shanghai, China). Briefly, rats were euthanized and immersed in 75% alcohol for 10 to 15 min, followed by detachment of the femur and tibia. Then, rBMSCs were collected from the bone shafts after the bone marrow was flushed out with α-MEM culture medium supplemented with 15% fetal bovine serum (FBS, Bovogen Biologicals Pty Ltd, Australia) and 100 IU/mL streptomycin/penicillin (HyClone, Thermo Fisher Scientific). In addition, RAW264.7 cells were cultured in a growth medium (DMEM with 15% FBS and 100 IU/

mL streptomycin/penicillin). The culture medium was refreshed every two to three days. rBMSCs at passage three and RAW264.7 cells with the indicated concentration (1×10^8 cells/mL) were prepared at 37 °C and 5% CO_2 for subsequent in vitro cytological experiments.

Cell Attachment

Cell attachment of rBMSCs in the hydrogel scaffolds was evaluated by a cell counting kit-8 (CCK-8) assay after 6 and 20 h of coculture.[25,26] A total of 100 μL of medium containing rBMSCs at a density of 1×10^5 cells/well was seeded into 96-well plates (Corning, Merck). Scaffolds with cells were gently rinsed with PBS twice to remove floating cells, and 50 μL of CCK-8 solution (Dojindo Molecular Technologies Inc., Kumamoto, Japan) was added to the wells after coculture for an additional 2.5 h incubation at 37 °C. The absorbance was confirmed at 450 nm (OD_{450}) on a spectrophotometer (Infinite M200 PRO, TECAN, Männedorf, Switzerland). In addition, rBMSCs grown on the hydrogel scaffolds were stained with 4.6-diamidino-2-phenylindole (DAPI, 10 μg/mL, Solarbio, Beijing, China) for 10 to 15 min, followed by visualization of nuclei using confocal laser scanning microscopy (CLSM, Leica TCS SP8, Leica Microsystems, Mannheim, Germany) observation.[8]

Cell Proliferation

To further investigate the effects of the hydrogel scaffolds on the proliferation of rBMSCs, a CCK-8 assay was also performed as described above. The inoculum density of rBMSCs was 1×10^4 cells/well, and the OD_{450} values were obtained after 1, 3 and 5 d of coculture. The relative proliferation rate of rBSMCs on Days 3 and 5 in each group was confirmed and compared after normalization to those on Day 1 to exclude the interference of inoculation discrepancy.[32]

Cell Viability and ROS Detection

To obtain a comprehensive assessment regarding the in vitro cytocompatibility of GO/Cu- functionalized hydrogel scaffolds, a Live/Dead Cell kit (Abcam, Cambridge, UK) was used after 24 h of coculture as previously indicated.[32] The procedures of cell inoculation were similar to those of cell attachment. rBMSCs in the hydrogel scaffolds were fixed with 4.0% neutral paraformaldehyde (PFA) for 15 min at room temperature, and then cells were stained with 100 μL of combination dye for 10 min. Stained samples were scanned and visualized by CLSM (Leica Microsystems) after being rinsed twice with PBS. Specifically, viable and apoptotic cells spread out over the hydrogel scaffolds demonstrated fluorescent green and red, respectively, according to the manufacturer's instructions. Moreover, the oxidative stress of rBMSCs in response to the hydrogel scaffolds was examined by a reactive oxygen species (ROS)-sensitive fluorescent probe, 2',7'-dichlorofluorescin diacetate (DCFH-DA), as reported in our previous work.[30] As a widely used probe to monitor cellular redox processes, DCFH-DA can react toward a broad range of oxidizing products during intracellular oxidant stress.[33] Briefly, rBMSCs in each well were stained with 100 μL of DCFH-DA (10 μM, Solarbio) for 30 min at 37 °C after 24 h of coculture, followed by three washes with PBS to remove excess dye outside the cells, and the fluorescent photos of stained samples were scanned and recorded by CLSM (Leica Microsystems). In addition, the ROS fluorescence intensity in each well was determined by a multidetector microplate reader (EnVision 2105, PerkinElmer, USA) at 488 nm (excitation wavelength) and 525 nm (emission wavelength) according to the provided manual.

Macrophage Polarization and Expression of Inflammatory Cytokines

In this study, the polarization of RAW264.7 cells and expression levels of inflammatory cytokines were evaluated by fluorescence staining and ELISA assay according to previous protocols.[12,34] To be brief, RAW264.7 cells at a density of 5×10^4 cells/well were seeded into 48-well plates containing hydrogels. After 48 h of coculture, the hydrogel scaffolds were fixed with 4.0% PFA for 15 min and permeabilized with 0.1% Triton-X (Solarbio) for 30 min, followed by 1 h blocking using 5% bovine serum albumin (BSA) blocking buffer (Solarbio). Cells grown in the hydrogels were sequentially incubated with M1 primary anti-CCR7 antibody (1:100, Abcam) at 4 °C overnight, secondary Alexa Fluor® 488 antibody (1:500, Abcam) for 2 h at room temperature, M2 primary anti-CD206 antibody (1:50, Abcam) at 4 °C overnight and finally secondary Alexa Fluor® 594 antibodies (1:500, Abcam) for 2 h at room temperature. Fluorescent images of stained hydrogels were scanned and recorded by CLSM (Leica Microsystems). In addition, the expression levels of typical pro-inflammatory (IL-1β and TNF-α) and anti-inflammatory (IL-4 and IL-10) cytokines were evaluated by corresponding enzyme-linked immunosorbent assay (ELISA) kits (Solarbio) according to the provided manufacturer's instructions. The OD_{450} values were recorded on a spectrophotometer (TECAN), and the final concentrations (pg/mL) of secreted inflammatory factors mentioned above were confirmed according to the fitted standard curves.

In vitro Osteogenic Differentiation

Cell Culture and Osteoblast Differentiation

rBMSCs were used to investigate the osteogenic potential of the hydrogel scaffolds according to previous protocols.[25,30] In summary, extraction liquid from the hydrogel scaffolds was obtained after one week of degradation in α-MEM solution at 37 °C under sterile conditions as described previously.[27,35] rBMSCs at a density of 4×10^5 cells/well were seeded into 12-well plates, followed by a refresh of culture medium specialized for osteogenic differentiation (OriCell, Cyagen Biosciences Inc., USA) after one day of cell attachment and spreading. The osteogenic induction medium containing hydrogel extractions was renewed every 2 to 3 d.

ALP Staining and Quantitative Determination

To determine the osteogenic effects of the hydrogel extractions on rBMSCs, an alkaline phosphatase (ALP) staining kit (Nanjing Jiancheng Bioengineering Institute, China) was used after 6 and 10 d of induction, and ALP-positive cells were visualized by a microscope (Leica Microsystems).[25] Then, a matched ALP microplate test kit (Nanjing Jiancheng Bioengineering Institute) was used to further confirm the ALP activity of each well according to the provided protocols. The quantity of ALP content in collected cell lysates was determined at 520 nm (OD_{520}) on a spectrophotometer (TECAN), followed by normalization to the corresponding total protein content (OD_{562}) measured by a BCA protein assay kit (Thermo Fisher Scientific). The relative ALP activity of rBMSCs in each well was finally expressed as the OD_{520}/normalized ALP protein content.

ARS Staining and Quantitative Determination

The in vitro mineralization of rBMSCs was investigated by an Alizarin Red S (ARS) staining kit (Cyagen Biosciences) after 21 and 28 d of induction as reported in our previous studies.[25,30] Cells were fixed with 4% PFA for 30 min after washing three times with PBS, and ARS staining working solution (pH = 4.2) was added to each well and incubated for approximately 1 h to visualize the calcium nodule formation of rBMSCs. Stained samples were washed thrice with PBS to remove unstained dye, and photographs were obtained by a microscope (Leica Microsystems). Then, 10% cetylpyridinium chloride in 10 mM sodium phosphate (Sigma-Aldrich) was added to the dried samples to quantify the ARS staining, and OD_{620} values in each well were measured on a microplate reader (TECAN).

Real-Time Quantitative PCR Evaluation of Osteogenic Differentiation-Associated Genes

In this study, real-time quantitative polymerase chain reaction (RT-qPCR) was conducted to observe the expression levels of osteogenic-associated genes, such as *ALP*, Runt-related transcription Factor 2 (*RUNX-2*), osteocalcin (*OCN*) and osteopontin (*OPN*), and the housekeeping gene glyceraldehyde-3-phosphate dehydrogenase (*GAPDH*) served as the internal control.[3,25,30] The specific primer sequences used for the qPCR analysis are shown in Table S1. rBMSCs at a density of 1×10^6 cells/well were seeded into 6-well plates, and the total RNA in each well was extracted by TRIzol reagent (Invitrogen, Thermo Fisher Scientific) after 6, 10 and 14 d of osteogenic induction according to the manufacturer's instructions. The concentration and purity of the collected RNA samples were confirmed by a NanoDrop spectrophotometer (ND-100, Thermo Fisher Scientific), followed by cDNA synthesis using a PrimeScriptTM RT reagent kit (Takara Bio Inc., Dalian, China). Then, prepared cDNA and specific primers were mixed with a TB Green® Premix Ex TaqTM kit to quantify the mRNA expression of osteogenesis-associated genes as mentioned above on a QuantStudioTM 7 Flex Real-time PCR System (Applied Biosystems, Thermo Fisher Scientific). The Ct value of each gene was documented and calculated through the comparative $2^{-\Delta\Delta}$Ct method.[3,36]

In vivo Neovascularization and Biocompatibility

Establishment of a Subcutaneous Implantation Model in Mice

To investigate the in vivo neovascularization and biocompatibility of GO/Cu-functionalized hydrogel scaffolds, we established a subcutaneous implantation model in mice as described previously.[37,38] The procedures for this animal experiment were reviewed and approved by the Laboratory Animal Welfare and Ethical Committee (IACUC) of Central South University (CSU-2022-0209). Twenty-four BALB/c mice (female, 25–30 g) purchased from Hunan Slac Jingda Laboratory Animal Co., Ltd. were adopted and randomly divided into four groups (G, G/T, G/T/GO and G/T/GO/Cu, n = 6 for each group) (Table S2). All mice received intraperitoneal anesthetization (1% pentobarbital sodium, 50 μg/g body weight) prior to the operation. Then, a dorsal incision (1 cm in length) parallel to the spine was made, and a subcutaneous pocket was created, followed by implantation

of one semicircular hydrogel scaffold (diameter × thickness: 7 mm × 4 mm) under the skin (Figure S1a). The surgical incisions were closed with 4–0 ETHICON sterile sutures. Mice were kept separately, and the application of analgesics and antibiotics postoperatively depended on the clinical observations under the IACUC recommendations. The mice were sacrificed at the indicated time points (2 and 4 weeks) after implantation, and the subcutaneous neovascularization of the hydrogel scaffolds was photographed and recorded by a digital camera before sampling.

Histological Evaluation and in vivo Biosafety

Following the observation of subcutaneous neovascularization, the hydrogel scaffolds and surrounding soft tissues were carefully excised from each mouse and fixed in 4% PFA for subsequent histologic processing. All the fixed samples (n = 3) were processed routinely for paraffin embedment and preparation of tissue sections (4 μm in thickness), followed by histological staining with hematoxylin and eosin (H&E) and Masson's Trichrome. In addition, several vital organs, including the heart, lung, liver, kidney and spleen, were harvested at corresponding sacrifice time points, and H&E staining was used to examine the organizational structures of these organs to validate the in vivo biosafety of the biohybrid hydrogel scaffolds after implantation.[25,30] More importantly, immunofluorescent CD31, F4/80 and CD3 staining were used to evaluate the neovascularization and macrophage and lymphocyte infiltration of the extracted hydrogel scaffolds, respectively, according to previously reported protocols.[26,38,39] In addition, dual immunofluorescent CD206/iNOS staining of the biohybrid hydrogel scaffolds was performed to clarify the in vivo effects of implanted hydrogel scaffolds on M1 (iNOS) and M2 (CD206) type polarization during macrophage recruitment. In brief, prepared slices were dehydrated sufficiently using xylene and graded ethanol (100%, 85% and 75%), then, blocking of nonspecific proteins was conducted using 3% BSA solution after antigen retrieval at room temperature for 30 min prior to the incubation of antibodies. Subsequently, the sections were incubated with primary antibodies (CD31, 1:3000, SAF005, AiFang Biological, Changsha, China; F4/80, 1:8000, SAF002, AiFang Biological; CD3, 1:2500, ab16669, Abcam; CD206, 1:3000, 24595, Cell Signaling Technology; iNOS, 1:1000, CL488-80517, Proteintech) overnight at 4 °C. Subsequently, the slices were incubated with secondary antibodies (ready-to-use, AFSA004, HRP-Goat Anti-Rabbit IgG, AiFang biological) for 1 h at room temperature. Finally, the nuclei of the tissue sections were counterstained with DAPI (1 mg/mL, C0060, Solarbio) for 10 min at room temperature. To determine the biological effects of hydrogel scaffolds on neovascularization, macrophage recruitment and lymphocyte infiltration, all stained sections were observed by a fluorescence microscope (Eclipse C1, Nikon, Tokyo, Japan), and images of five randomly selected fields around the implanted scaffolds were captured from the panoramically scanned fluorescent photograph using CaseViewer (version 2.4, Budapest, Hungary) and KFBIO digital slide viewer software (version 1.7.1.6, Ningbo, China). In addition, quantitative analysis of CD31+ new vessels and F4/80+ or CD3+ cells in each randomly selected field was performed using ImageJ software (NIH, Maryland, USA).

In vivo Bone Reconstruction Efficacy

Establishment of a Calvarial Bone Defect Model in Rats

To further validate the therapeutic efficacy of GO/Cu-functionalized hydrogel scaffolds in bone reconstruction, a modified calvarial bone defect model in rats was established according to previously published procedures.[6,31,40] The animal experiments reported herein were evaluated and approved by the Laboratory Animal Welfare and Ethical Committee (IACUC) of Central South University (Nos. CSU-2022-0209). Forty-eight SD rats (male, 200–250 g) purchased from Hunan Slac Jingda Laboratory Animal Co., Ltd. were used and randomly allocated into four groups (CTRL, G/T, G/T/GO and G/T/GO/Cu, n = 12 for each group) (Table S2). Anesthesia was induced by intraperitoneal anesthetization (1% pentobarbital sodium, 80 mg/kg body weight), and the surgical region was shaved and disinfected. Then, a longitudinal incision (2 cm in length) was made on the middle of the scalp, and the surface of the calvarium was exposed after stripping of the periosteum layer, followed by the formation of two circular full-thickness defects (4.5 mm in diameter) at the bilateral site of the calvarial sagittal suture using a slow-speed electric trephine drill. Subsequently, two sterile circular hydrogel scaffolds (diameter × thickness: 5 mm × 1 mm) were implanted into each of the separate defects (Figure S1b). The surgical incisions were closed with 4–0 ETHICON sterile sutures. All the experimental rats were kept separately, and the application of analgesics and antibiotics after surgery depended on the clinical observations under the IACUC recommendations. The rats were sacrificed at the indicated time points (6 and 12 weeks) after implantation, and the skull specimens were harvested and fixed in 4% PFA for subsequent micro-CT analysis and histological evaluation.

Micro-CT Scanning of Bone Defects

In situ bone regeneration induced by the implanted GO/Cu-functionalized hydrogel scaffolds in the abovementioned calvarial bone defect model was assessed by micro-CT scanning (μCT 100, Scanco Medical, Brüttisellen, Switzerland) with a pixel resolution of 30 μm at 6 and 12 weeks (n = 3 for each time point) postoperatively.[41,42] The voltage and current of the scanning were 70 kV and 200 μA, respectively. In addition, representative 3D-reconstructed images and corresponding sagittal sections were obtained, and relevant morphometric data, including bone volume/total volume (BV/TV) and bone surface/total volume (BS/TV), of the region of interests (ROIs) in bone defect sites were recorded and analyzed by the provided manufacturer's processing software (Image Processing Language, Scanco Medical AG).

Histological Evaluation and in vivo Biosafety

The skull specimens (n = 3) containing ROIs as described in micro-CT scanning were processed for histological staining after samples were decalcified in 10% EDTA for approximately three to four weeks.[6,41] The routine procedures for paraffin embedment and preparation of tissue slices (4 μm in thickness) were similar to the abovementioned protocols, and selected slices at the mid-sagittal plane of the defect region were stained with H&E and Masson's trichrome to observe bone healing.[40] Similarly, several vital organs, including the heart, lung, liver, kidney and spleen, were also harvested and stained with H&E to examine the organizational structures of these organs to validate the in vivo biosafety of the biohybrid hydrogel scaffolds after 6 and 12 weeks of implantation. Meanwhile, immunofluorescent CD31 (1:3000, SAF005, AiFang Biological), OCN (1:100, GB11233-100, Servicebio, Wuhan, China) and OPN (1:2500, AF07486, AiFang Biological) staining was applied to investigate the angiogenesis and bone regeneration-associated specific proteins within the defect areas,[41,43,44] and the procedures involved in the dehydration, serum blocking, antibody incubation of prepared slices were basically consistent with the previously mentioned contents. All stained sections were observed by a fluorescence microscope (Nikon), and images of five randomly selected fields within the bone defect regions were captured from the panoramically scanned fluorescent photograph using CaseViewer software. Quantitative analysis of CD31+ new vessels and OCN+ or OPN+ cells in each randomly selected field was performed using ImageJ software.

Statistical Analysis

All data are expressed as the mean ± standard deviation (mean ± SD) and were analyzed by Origin 8 (Origin Lab, MA, USA) or GraphPad Prism 5 software (GraphPad Software, CA, USA). One-way analysis of variance (ANOVA) with Tukey's post hoc test or nonparametric tests (Kruskal–Wallis *H*-test) were applied to conduct the statistical analysis with the assistance of SPSS software (version 24.0, IBM Corp, NY, USA) according to the determination of the normal distribution and homogeneity of variance. In addition, $p < 0.05$ was considered statistically significant and the specific p values were marked on corresponding diagrams.

Results and Discussion

Preparation and Characterization of the Biohybrid Hydrogel Scaffolds Incorporated with GO/Cu Nanosheets

Prior to the preparation of biohybrid hydrogel scaffolds, GO/Cu nanosheets were synthesized by an in situ chemical reduction method as mentioned in our previous works.[25,26] It has been suggested that CuNPs with a diameter of approximately 15 to 20 nm and good crystallinity were homogeneously captured on the surface of GO nanosheets due to electrostatic attraction and coordination.[25,45] Attributed to the in situ adsorption and bonding between copper ions and surface-charged oxygen-containing groups of GO nanosheets, sustainable release of copper (CuNPs/Cu^{2+}) from the GO/Cu nanocomposites is expected when designing metal ion-incorporated BTE scaffolds to combat bone defects.[24] Then, a photocrosslinking technique was conducted to prepare GO/Cu nanosheet-integrated hydrogel scaffolds after irradiation for 20 to 30s by blue light (405 nm) (Figure 1a). [17,27] Accompanied by the addition of β-TCP, GO nanosheets and GO/Cu nanocomposites, the transparent GelMA hydrogel scaffolds became muddy and brown accordingly (Figure 1a). The sponge-like structures of the prepared hydrogel scaffolds were observed by SEM, as shown in Figure 1b, and all the prepared scaffolds had an interconnected pore structure. The average pore sizes of the G, G/T, G/T/GO and G/T/GO/Cu scaffolds were 133.68 ± 47.23 μm, 228.42 ± 65.00 μm, 207.55 ± 59.94 μm and 175.70 ± 40.56 μm, respectively (Figure 1c). Moreover, the porosities of the hydrogel scaffolds were 72.24 ± 5.31%, 62.93 ± 1.64%, 65.16 ±

2.26% and 68.58 ± 1.40% for G, G/T, G/T/GO and G/T/GO/Cu, respectively, and the porosity of the G/T scaffold was significantly less than that of the G and G/T/GO/Cu scaffolds (Figure S2). Notably, with the addition of ingredients, the pore size of GelMA-based hydrogel scaffolds increased, which could facilitate cell adherence and growth into the scaffolds,[4] and appropriate micropore size and porosity are of significance when assembling biomimetic engineered scaffolds with the simulative structure of bone trabeculae.[10] In addition, the element distributions of the porous scaffolds determined by EDS indicated the exclusive existence of copper over the surface of the G/T/GO/Cu scaffold (Figure S3). These results confirmed the successful synthesis of the GO/Cu-functionalized GelMA/β-TCP hydrogel scaffold with typical porous microstructure.

In addition to the SEM observations, the surface topography of the biohybrid hydrogel scaffolds was further confirmed by high-definition laser microscopy (Figure 2). According to the 3D topographic images and quantitative analysis of the surface profile distribution, the surface roughness of GO/Cu-decorated scaffolds was significantly increased compared with that of pure GelMA scaffolds, probably due to the assembly and aggregation of GO/Cu nanocomposites that improved the microrough structure of the hydrogel scaffolds. Bioengineered materials with adequate microroughness provided favorable interfaces for cell adherence, spreading and osteogenic differentiation, therefore contributing to better initial cell–scaffold interactions and subsequent osseointegration or bone ingrowth.[46] The static water contact angles (WCAs) of the hydrogel scaffolds were measured to confirm the hydrophilicity or wettability of the material interfaces (Figure 3a and b). Clearly, the WCA of the GelMA scaffolds decreased significantly after incorporation of β-TCP, GO and GO/Cu, and the WCA of the G/T/GO scaffolds was also less than that of the G/T and G/T/GO/Cu scaffolds, indicating an evident improvement in the hydrophilicity of the modified composite scaffolds. Implanted biomaterials with increased hydrophilicity had a positive effect on the early stages of the attachment, spreading and proliferation of osteogenic cells,[47,48] thus providing a favorable cell-anchoring site for the rBMSCs in the cell-scaffold coculture system of this study. Undoubtedly, the biological behavior of cells is affected by numerous surface properties, such as morphology, roughness, surface energy, hydrophilicity and protein adsorption,[49] and the synthetic actions of these features on rBMSCs need to be further investigated in versatile in vitro and in vivo models.

Then, FT-IR and XPS were used to confirm the variation in bonds and elements in the hydrogel scaffolds after modification (Figure 3c and d). The absorption bands at 1100 cm^{-1}, 1650 cm^{-1} and 3300 cm^{-1} were related to oxygen-containing groups, such as OH-, COO- and C=O from GelMA substrates or GO nanosheets.[26,27] In addition, the absorption peak at 1520 cm^{-1} represented amide II bonds (N-H stretching), and the C=C stretching absorption peak representative of the methacrylate vinyl group at 1640 cm^{-1} was concealed by the strong amide I (C=O stretching) in GelMA.[50] Consistent with the EDS results, a typical Cu 2p peak at approximately 930 eV was only recorded in the GO/Cu-decorated hydrogel scaffolds,[25] and other typical peaks representing the corresponding valence states of elements were also found in the hydrogel scaffolds. Therefore, GO/Cu-incorporated hybrid hydrogel scaffolds were successfully synthesized after sufficient agitation and photocrosslinking procedures. The thermal degradation behavior of the hydrogel scaffolds ranging from 30 to 1100 °C was determined by TGA (Figure 3e). In short, there were four stages involved in the thermal degradation of all the tested hydrogel scaffolds. First, a weight loss of approximately 10% to 15% was recorded below 150 °C due to moisture evaporation within the scaffolds.[26] Second, an approximately 35% to 45% loss in weight was found ranging from 200 to 400 °C, which constituted the major decomposition of the hydrogel scaffolds due to cleavage of intermolecular bonds, oxygenated functional groups and molecular structures in GelMA and GO.[26] Third, a further loss in weight measured at 12% to 15%, ranging from 400 to 900 °C, was observed, which may be attributed to the further decomposition of the graphitic portion.[25] Eventually, a gradual decline measured at 13% to 15% after 900 °C was found in all the tested hydrogel scaffolds until the end of the TGA. Overall, a residual weight of 15% in the G/T/GO and G/T/GO/Cu scaffolds and 20% in the G and G/T scaffolds was calculated, and this discrepancy was closely related to the incorporation of GO and GO/Cu nanomaterials and detection limitations. Considering the significant role of the porous structure and swelling property of hydrogel scaffolds in regulating nutrients and gas exchanges for cell growth and proliferation,[4,43] the water absorption capacity of the scaffolds was determined by calculating the swelling ratio, as demonstrated in Figure 3f. There were no significant differences among the four groups regarding the swelling ratios at corresponding time points, and the average swelling ratios of these scaffolds were 719%, 980% and 1013% at 2, 24 and 48 h, respectively. Interestingly, the swelling ratio of our study was obviously greater than that the welling ratio reported in several previous works,[4,27,43] possibly due to different degrees of dehydration and material compositions of the used hydrogels. Additionally, the weight of these hydrogels reached a balance and saturation status after 48 h of immersion, signifying the good stability of the GO/Cu-decorated hydrogel scaffolds.

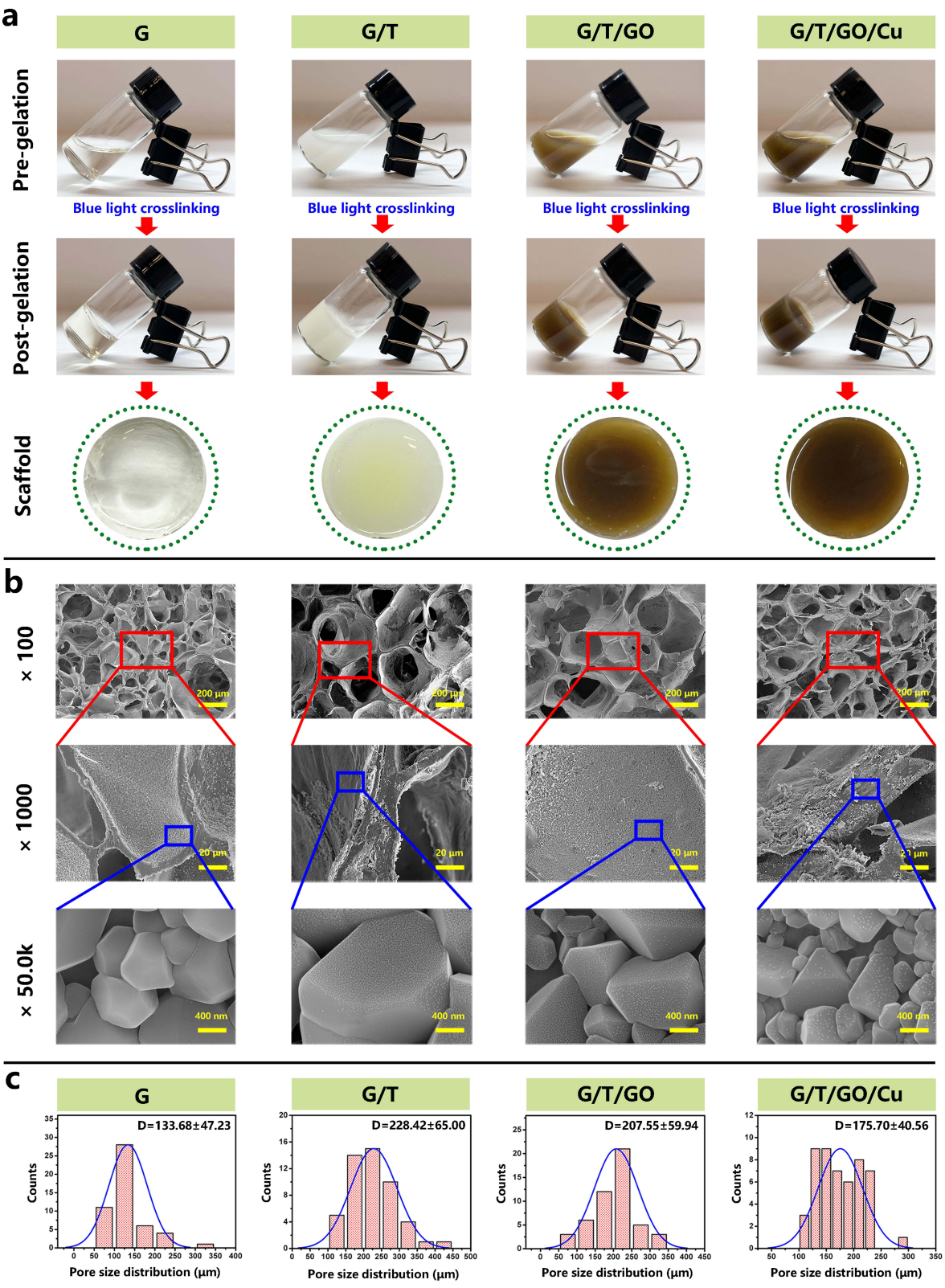

Figure 1 Gelation and morphology characterization of the biohybrid hydrogel scaffolds incorporated with GO/Cu nanosheets.
Notes: (a) Digital images of mixed solutions, hydrogels and prepared scaffolds. Gelated scaffolds were obtained after being irradiated by a portable blue light source (3 W, 405 nm) for 20 to 30s. **(b)** SEM images showing the porous microstructure of the hybrid hydrogel scaffolds. **(c)** Pore size distribution of various hydrogel scaffolds.
Abbreviations: GO/Cu, copper nanoparticle-decorated graphene oxide nanosheets; SEM, scanning electron microscope.

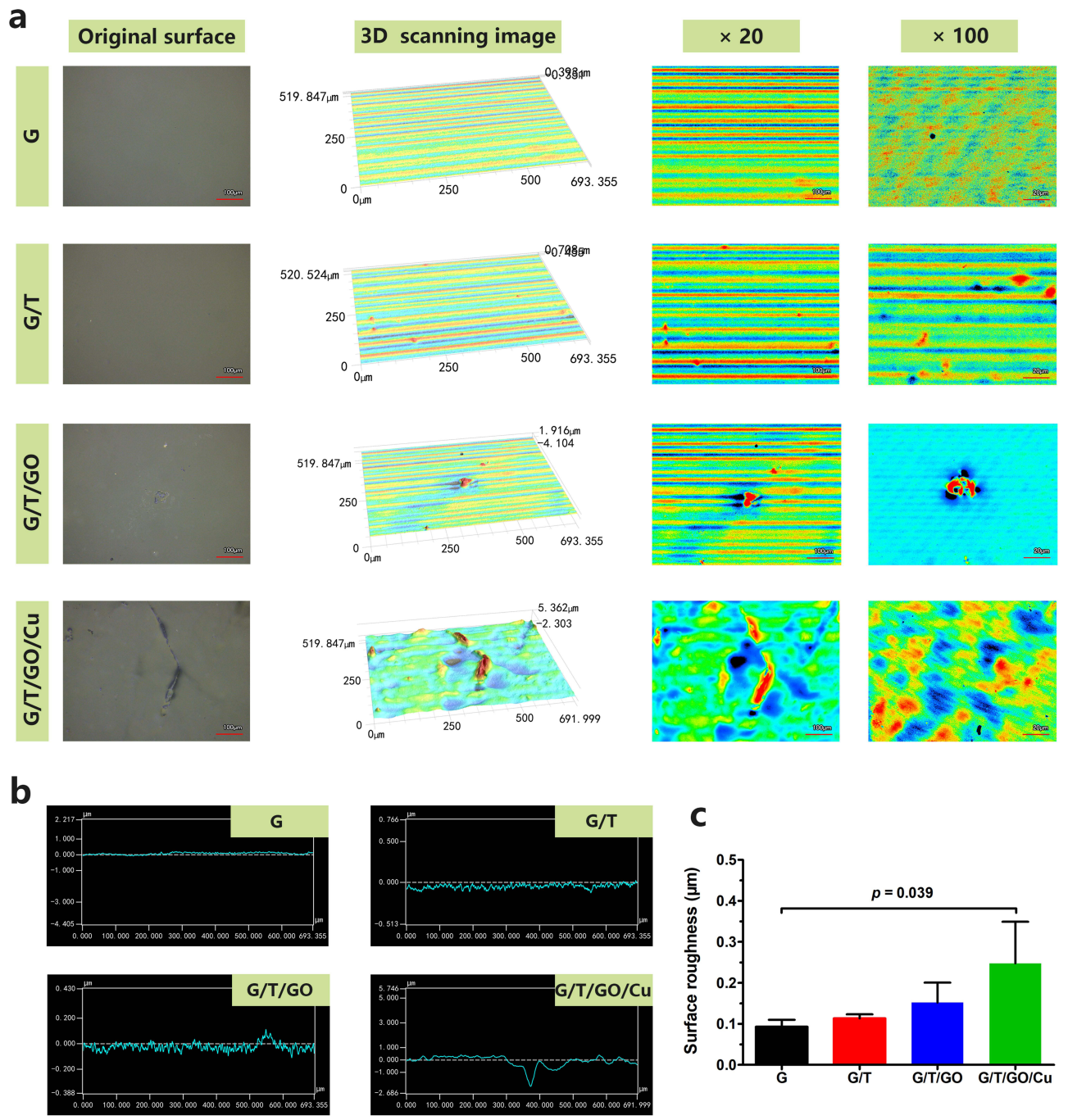

Figure 2 Three-dimensional laser microscopy showing the surface topography of the biohybrid hydrogel scaffolds.
Notes: (a) Representative 3D laser scanning images. **(b)** Record of surface profile distribution. **(c)** Quantitative analysis of the surface roughness.
Abbreviation: 3D, three-dimensional.

Considering the pH-dependent property of copper release from bioengineered substitutes, as confirmed previously,[26] in this study, the in vitro release kinetics of copper ions from the GO/Cu-integrated hydrogel scaffolds were also determined at different pH values (5.5, 7.4 and 8.5) for three weeks, as shown in Figure 3g. An initial burst release of Cu^{2+} from the GO/Cu-incorporated hydrogel scaffolds was found in all three groups with different pH values within 5 d of in vitro degradation, and the release amounts of Cu^{2+} from the hydrogels during this early stage were 50.3%, 41.1% and 31.7% in acidic, neutral and alkaline microenvironments, respectively. Subsequently, a relatively slow release of Cu^{2+} from the hydrogels was observed for all three groups until the end point of degradation, which demonstrated total release amounts of 66.5%, 55.2% and 47.5% with increasing pH values from 5.5 to 8.5, respectively. Our results showed that

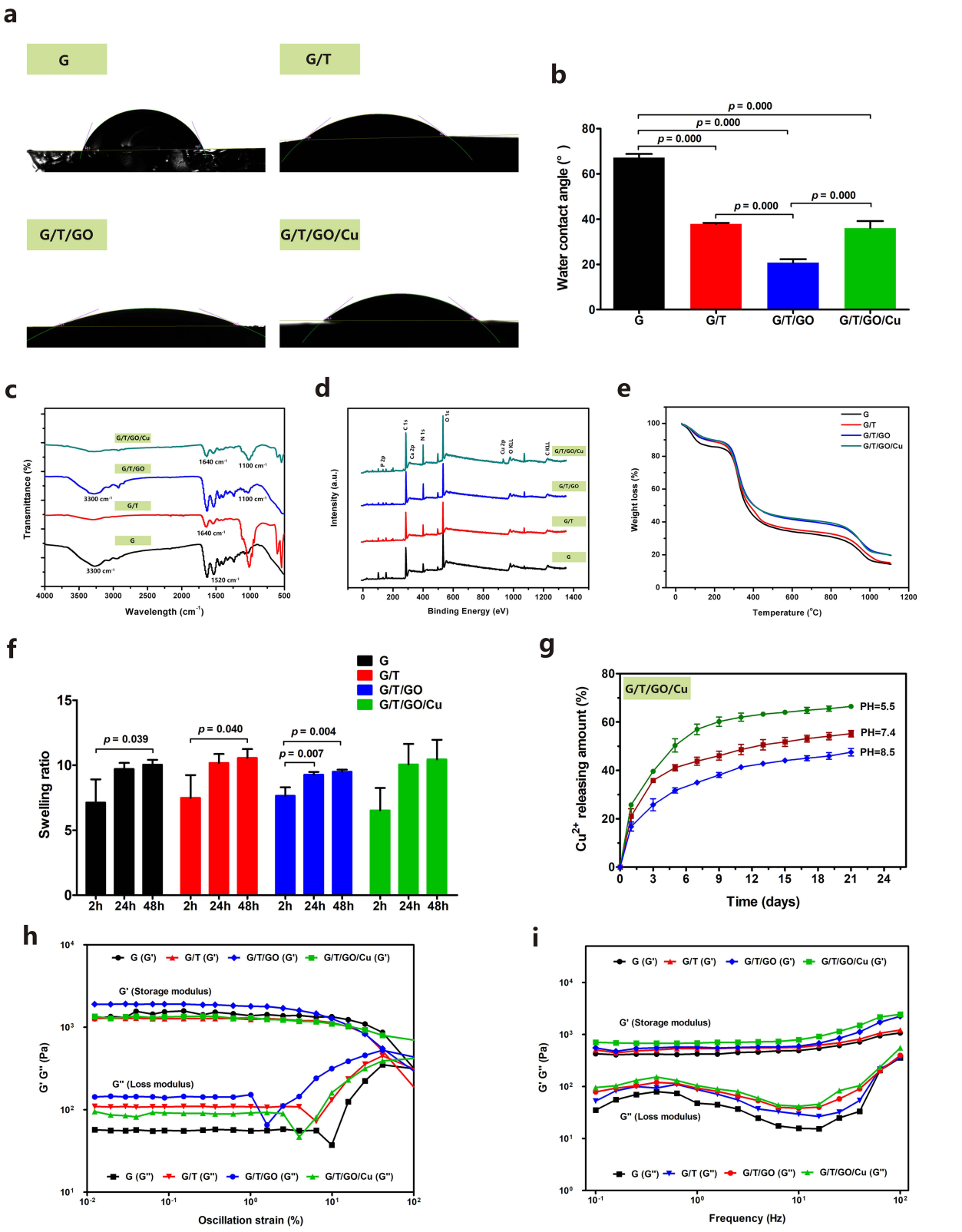

Figure 3 Morphological, chemical and physical characterizations of the biohybrid hydrogel scaffolds.

Notes: (a) Water droplets and **(b)** contact angles on the surface of the hydrogel scaffolds. **(c)** FT-IR spectra. **(d)** XPS survey spectra. **(e)** TGA analysis of the hydrogel scaffolds (10 °C/min, 30 to 1100 °C). **(f)** Swelling property of the hydrogel scaffolds after immersion in ddH_2O for 2, 24 and 48 h. **(g)** Cumulative release curves of copper ions from the GO/Cu-integrated hydrogel scaffolds at various pH values over three weeks recorded by ICP-OES. Rheological properties of the biohybrid hydrogel scaffolds determined by **(h)** oscillatory strain sweep measurement (0.1% to 100% strain) and **(i)** frequency sweep measurement (0.1 to 100 Hz).

Abbreviations: FT-IR, Fourier transform infrared spectroscopy; GO/Cu, copper nanoparticle-decorated graphene oxide nanosheets; ICP-OES, inductively coupled plasma-optical emission spectrometry; TGA, thermogravimetric analyzer; XPS, X-ray photoelectron spectroscopy.

approximately half of the loaded copper was retained after three weeks of in vitro release in GO/Cu-incorporated hydrogel scaffolds under neutral and alkaline conditions, suggesting a conceivable long-lasting in vivo release in the calvarial bone defect model resulting in better copper ion-induced osteogenesis and bone regeneration under aseptic conditions. Repairing acute or chronic bone infections is still a great therapeutic challenge, and an acidic environment caused by tissue necrosis and active metabolism of colonized bacterial cells or biofilms was found in these bacteria-infective scenarios, making it feasible and effective to design a pH-sensitive sustained release platform for anti-infection and osteogenesis purposes.[51,52] Combining the excellent responsive properties of hydrogels toward temperature or pH, these GO/Cu-incorporated hydrogel scaffolds may also be suitable for repairing bacteria-contaminated bone injury, which will be further investigated in our future works. Furthermore, the in vitro biodegradation properties of the hydrogels were determined as shown in Figure S4 which indicated that all the tested hydrogel scaffolds were biodegradable with the treatment of collagenase that exists in the repairing microenvironment of tissues.[28] The G and G/T/GO hydrogels exhibited a residual mass of approximately 90% after 4 days of enzymatic degradation, and the residual mass of G/T/GO/Cu hydrogels was still 90% at day 10. To the contrary, the G/T hydrogels exhibited a remarkable increased degradation rate from day 5 to 14 compared with other groups. These results implied that the addition of β-TCP nanoparticles breaked the crosslinking stability of pure GelMA hydrogels, and the combination of GO nanosheets and copper nanoparticles reinforced the enzymatic degradation stability of pure GelMA, which may be caused by the potential electrostatic interaction of nanocomposites within the gel networks. The degradation rate of the hydrogels was significantly reduced after incorporation of copper ions, which was similar to a previously reported work,[29] and the deceleration of enzymatic degradation would facilitate the biological activity of the hydrogels during early stage of bone healing.

In addition, the rheological properties of the prepared hydrogel scaffolds were confirmed by strain and frequency sweep measurements to evaluate the potential effects of incorporated GO or GO/Cu nanomaterials on the mechanical properties of the hydrogel scaffolds as previously described.[3,4,43] The linear viscoelastic networks of the hydrogel scaffolds were investigated by recording the change in storage (G′) and loss (G″) modulus, and G′ > G″ represents the gel state for the tested samples.[3] Overall, the four types of hydrogel scaffolds exhibited similar rheological behaviors in the two different detection models. The values of G′ and G″ obtained from these hydrogels were constant with G′ > G″ during the oscillation strain range of 0.01% to 50%, except for several low amplitude variations that occurred within 1% to 10% (Figure 3h). Then, the viscoelasticity of the hydrogel scaffolds was also clarified by performing a frequency scanning method with frequencies ranging from 0.01 to 50 Hz, as shown in Figure 3i. Clearly, the incorporation of GO/Cu nanocomposites increased the storage modulus of the biohybrid hydrogels, which may improve the deformation resistance of hydrogels. Meanwhile, the G′ of each group was greater than G″ within the tested frequency range, indicating a satisfactory stability of the three-dimensional networks of the prepared hydrogels. According to the results of the swelling and rheological properties of the hydrogels with an interconnected pore structure, analyzed above, these GO/Cu-integrated hydrogel scaffolds are expected to be applicable substitutes that can be appropriately implanted into the defect regions created in rat calvarial bone to achieve accelerated bone healing and regeneration.

In vitro Cytocompatibility with rBMSCs of the Biohybrid Hydrogel Scaffolds

Clarifying the cytocompatibility and biocompatibility before actual application in tissue engineering and clinical scenarios is of great significance.[25,26] In this study, a series of in vitro experiments, such as cell adherence, proliferation, viability and oxidative stress response, were performed to comprehensively evaluate the cytocompatibility of the GO/Cu-incorporated biohybrid hydrogel scaffolds with rBMSCs (Figure 4). First, the attachment of rBMSCs grown over the surface of hydrogel scaffolds was confirmed by CCK-8 assay and DAPI staining after 6 and 20 h of coculture (Figure 4a and b). Quantitative determination of absorbance and CLSM observation of nuclear staining showed no significant differences among inoculated rBMSCs on the four different hydrogels, and the number of adhered cells increased prominently with the extension of incubation time. In addition, cell proliferation of rBMSCs was investigated using a CCK-8 assay after 1, 3 and 5 d of coculture, as shown in Figure 4c. In accordance with the results of cell adherence, there were no obvious differences in cell proliferation among the four groups at each time point, and the attached live cells demonstrated a steady growth trend within 5 d of cocultivation, indicating that the GO/Cu-integrated hydrogel scaffolds provided a favorable honeycomb-like microenvironment for sequential cell attachment and proliferation, which laid an important foundation and prerequisite for subsequent in vitro osteogenic differentiation and in vivo osseointegration.[30] To further investigate the potential cytotoxicity of GO/Cu-integrated hydrogel scaffolds, the viability of

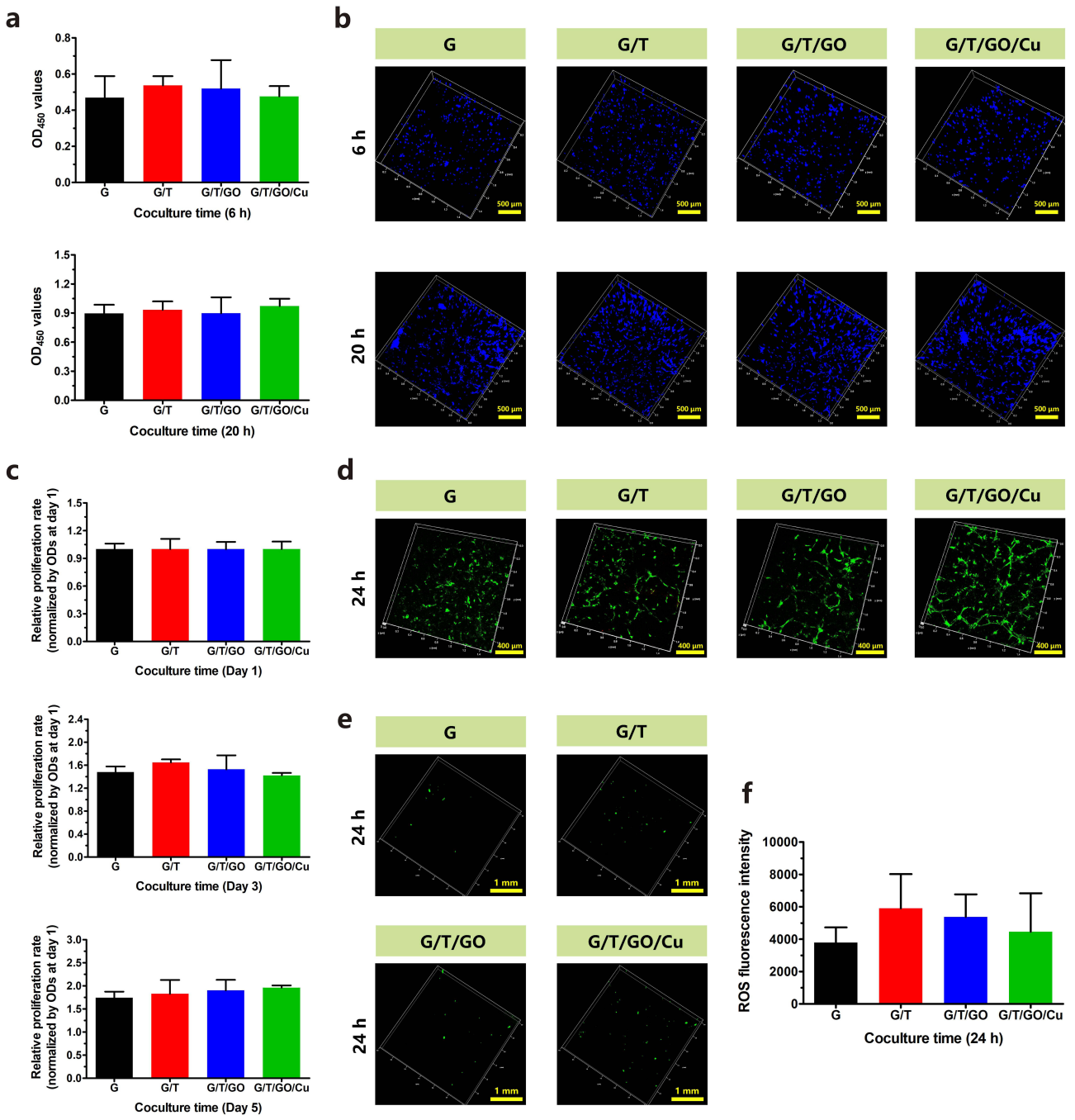

Figure 4 Investigation of the cytocompatibility of the biohybrid hydrogel scaffolds with rBMSCs.
Notes: (a) Cell attachment as confirmed by CCK-8 assay and **(b)** DAPI staining after 6 and 20 h of coculture. **(c)** Cell proliferation as confirmed by CCK-8 assay after 1, 3 and 5 d of coculture. **(d)** Cell viability determined by CLSM observation using live/dead cell staining after 24 h of coculture. **(e)** CLSM observation and **(f)** fluorescent quantitative analysis of oxidative stress (ROS) in rBMSCs in response to different hydrogel scaffolds after 24 h of coculture.
Abbreviations: CCK-8, cell counting kit-8; CLSM, confocal laser scanning microscopy; DAPI, 4.6-diamidino-2-phenylindole; rBMSCs, rat bone mesenchymal stem cells; ROS, reactive oxygen species.

rBMSCs grown on various hydrogel scaffolds was confirmed by CLSM observation after cells were stained by a live/dead cell staining kit (Figure 4d). The rBMSCs displayed good viability with few dead cells in the four groups, and the spreading and cytoskeleton of cells grown on the GO nanosheet-incorporated hydrogels (G/T/GO and G/T/GO/Cu) were distinctly better than those of cells grown on the G and G/T hydrogels. Our results indicated that the addition of GO-based nanomaterials facilitated cell spreading without detrimental cell apoptosis, and the biological effects of these GO-based hydrogels on cell behaviors (attachment, proliferation and spreading) could be modulated by regulating the physical performance and GO or GelMA concentration

of the biohybrid hydrogel scaffolds.[53] Moreover, ROS regeneration within the rBMSCs cocultured with different hydrogel scaffolds was visualized after staining with a DCFH-DA fluorescent probe (Figure 4e and f). Notably, relatively sparse green fluorescence was recorded in all the groups, followed by quantitative confirmation of ROS fluorescence intensity, indicating a significantly low level of free radicals (such as O_2•-, H_2O_2 and •OH) accumulated in rBMSCs after coculture with the hydrogels.[17,30] As an essential trace element in human biological systems, copper plays a critical role in enzymatic homeostasis and cytokine function; however, GO or copper at high concentrations may unavoidably induce apoptosis and autophagy in mammalian cells, hampering the normal biological behaviors of rBMSCs in the coculture system.[54,55] Based on the improvement and optimization of the biocompatibility of the GO-based platform by our research team,[25,26,30] the balance between the cytotoxicity and bioactivities regarding the GO/Cu nanoderivatives with different mass ratios and concentrations was virtually certain, which was also verified in the present biohybrid hydrogel system. In summary, the biohybrid hydrogel scaffolds exhibited good cytocompatibility with rBMSCs, and the incorporation of GO/Cu nanocomposites into the GelMA/β-TCP matrix serving as a bone substitute is expected to promote osteogenic potential, accelerate bone regeneration and achieve satisfactory biosafety, as discussed later.

In vitro Macrophage Polarization of RAW264.7 Cells of the Biohybrid Hydrogel Scaffolds

Considering the pivotal role of macrophage functions in bone tissue regeneration,[12,13] we further investigated the macrophage polarization (M1/M2) and expression of relevant inflammatory cytokines (IL-1β, TNF-α, IL-4 and IL-10) in the hydrogel scaffolds after 48 h of coculture. As shown in Figure S5a, the expression of M1 (CCR7) and M2 (CD206) markers in RAW264.7 macrophages cocultured with the hydrogel scaffolds was determined using fluorescence staining. It was found that the fluorescence intensity of CCR7 was relatively low in all the four groups, whereas the fluorescence intensity of CD206 was significantly increased in the G/T/GO/Cu hydrogels compared with that in the other three groups, indicating that the incorporation of GO/Cu nanocomposites into the GelMA hydrogels induced M2 type macrophage polarization. Moreover, all the prepared hydrogel scaffolds exhibited no significant effects on the M1 type macrophage polarization, especially in G/T/GO/Cu hydrogels. In general, M1 macrophages induce inflammatory response with release of IL-6, IL-1β and TNF-α, whereas M2 macrophages induce anti-inflammatory response with release of TGF-β, IL-4 and IL-10.[12,34] To further investigate the osteoimmunological property of the GO/Cu-decorated biohybrid hydrogels, the expression levels of typical inflammatory cytokines were confirmed by ELISA (Figure S5b). The pro-inflammatory cytokines (IL-1β and TNF-α) exhibited no significant differences among the four groups, except that the expression of IL-1β in G/T/GO hydrogels was higher than that in the G and G/T/GO/Cu hydrogels. In contrast, the expression of anti-inflammatory cytokines (IL-4 and IL-10) in G/T/GO/Cu hydrogels was significantly upregulated compared with the other three groups. These results indicated that the GO/Cu-decorated hydrogels could induce M2 type polarization in macrophages, followed by inhibited inflammatory reaction. Macrophages are usually activated and polarized to an M1 phenotype in the early stage of inflammation caused by injury or infection,[34] and the increased ratio of M2/M1 type macrophages could further promote the osteogenic differentiation of BMSCs.[12,56] Thus, implanted substitutes (G/T/GO/Cu hydrogels) with osteoimmunomodulatory function that induce M2 phenotype of macrophages provide favorable microenvironment to realize better bone tissue healing and remodeling. More importantly, our results showed that the interconversion of M1/M2 phenotype relied largely on the copper ions released from the hybrid hydrogels,[57] which may contribute to the subsequent osteogenesis and angiogenesis as discussed latter, leading to decreased inflammation-induced damage and accelerated bone repair.

In vitro Osteogenic Bioactivity of the Biohybrid Hydrogel Scaffolds

Aside from cytocompatibility, the osteogenic capability of implanted scaffolds is essential for achieving the desired in situ bone regeneration at defect sites.[27] Therefore, the osteoinductive activity of the GO/Cu-decorated biohybrid hydrogel scaffolds was determined by coculturing rBMSCs with hydrogel extracts from different groups in osteogenic induction medium for nearly one month. As shown in Figure 5a and b, the early and late markers of in vitro osteogenesis were evaluated by qualitative and quantitative analysis of ALP and ARS staining, respectively.[4,43] Compared to the pure GelMA hydrogel, the staining density of the G/T, G/T/GO and G/T/GO/Cu hydrogels was evidently enhanced at the indicated coculture time points, and the corresponding

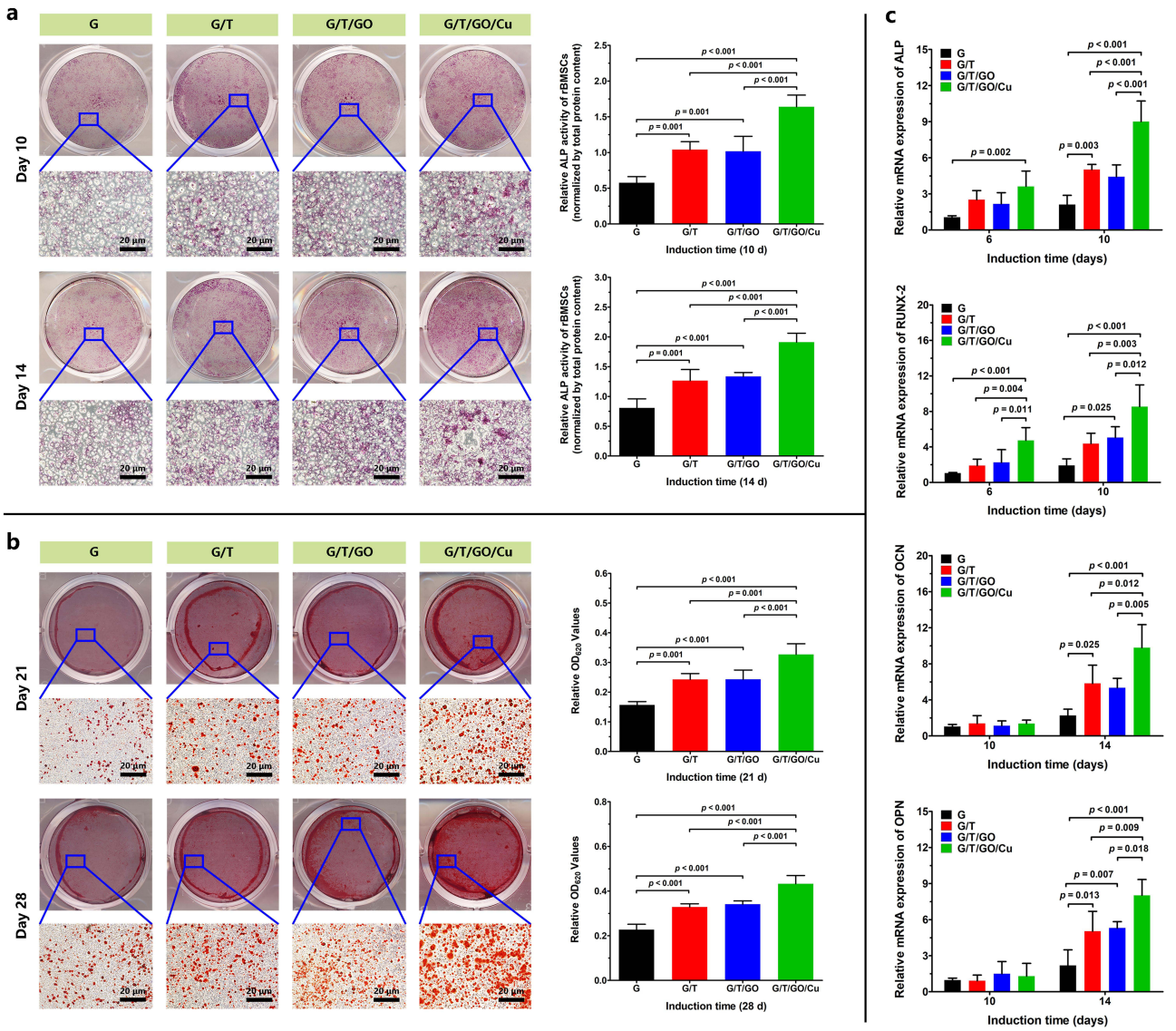

Figure 5 The osteogenic properties of extracts from the biohybrid hydrogel scaffolds.

Notes: (a) ALP staining and ALP activity of rBMSCs after 10 and 14 d of osteogenic induction. **(b)** ARS staining and mineral deposition determination after 21 and 28 d of osteogenic induction. **(c)** Relative mRNA expression of osteogenic genes (*ALP, RUNX-2, OCN* and *OPN*) as confirmed by real-time PCR after 6, 10 and 14 d of osteogenic induction.

Abbreviations: ALP, alkaline phosphatase; ARS, Alizarin Red S; mRNA, messenger ribonucleic acid; OCN, osteocalcin; OPN, osteopontin; PCR, polymerase chain reaction; RUNX-2, Runt-related transcription factor 2.

reaction color became darker with increasing induction time, indicating that the incorporation of β-TCP and GO or GO/Cu nanomaterials promoted the osteogenic activity of the pure GelMA hydrogel scaffold. To further elucidate the possible mechanism underlying the osteogenic responses of rBMSCs in the hydrogel-cell coculture system, the expression of several typical osteogenic-associated marker genes, such as *ALP, RUNX-2, OCN* and *OPN*, was confirmed by real-time PCR after 6, 10 and 14 d of induction (Figure 5c). Consistent with the findings of ALP and ARS staining, the expression of these genes in the early (*ALP* and *RUNX-2*) and late (*OCN* and *OPN*) stages of osteogenic differentiation observed in the G/T, G/T/GO and G/T/GO/Cu hydrogels was significantly greater than that in pure GelMA, and the G/T/GO/Cu hydrogels had the highest gene expression compared to that in the other groups.

Despite the excellent biocompatibility, degradation and tunable mechanical properties of GelMA, combining GelMA and bioactive materials with outstanding osteogenic capability to obtain better osteoregenerative potential of currently used composites is still essential.[16–18] β-TCP is a suitable candidate for synthesizing BTE scaffolds due to its nontoxicity, good biocompatibility and bioabsorbability, and the release of calcium and phosphorus ions from β-TCP also contributes

to the improvement of the osteogenic capacity of hydrogel scaffolds.[4] The introduction of GO into hybrid scaffolds could promote cell attachment, migration, proliferation and differentiation of osteoblasts;[21–23] however, no significant differences were found between the G/T and G/T/GO hydrogels in terms of the in vitro enzyme activity of ALP and formation of calcified nodules. The underlying reasons for this finding may be discrepancies in the composition, porosity, rheology and degradation of the used hydrogel systems, and the actual and extended impacts of the incorporated GO nanosheets within hydrogels on osteogenesis remain to be further explored in animal models. Inspired by the excellent osteogenic activity of GO-based nanomaterials and copper ions, as previously confirmed,[21,24] in this study, we found that the combination of β-TCP nanoparticles and GO/Cu nanocomposites exhibited a synergetic effect on promoting the osteogenic differentiation of rBMSCs, and the ECM-like microenvironment of the prepared hydrogel scaffolds facilitated the physiological process of bone matrix and mineralization. Collectively, this GO/Cu-integrated biohybrid bone substitute with good cytocompatibility, reduced cytotoxicity, osteoimmunomodulatory function and improved osteogenic capability provides a favorable matrix environment for subsequent in vivo new bone formation and bone tissue remodeling.

In vivo Neovascularization and Biocompatibility of the Biohybrid Hydrogel Scaffolds

Prior to the validation of bone repair capability, we established a subcutaneous implantation model in mice to investigate the in vivo neovascularization and biocompatibility of GO/Cu-functionalized hydrogel scaffolds according to previous reports with modifications (Figure 6a).[37,38] Appropriate vascular network formation is essential for acquiring indispensable nutrient substances and metabolite excretion to generate new multifunctional tissues, which contribute to vascularized bone regeneration.[3,10] The mice were sacrificed at 2 and 4 weeks after implantation, and subcutaneous neovascularization of the hydrogel scaffolds was photographed and recorded as demonstrated in Figure 6b. Significantly more newly formed vessels were found around the G/T/GO/Cu hydrogel scaffold compared to the other three groups, indicating that released copper ions from GO/Cu nanocomposites incorporated into the hydrogels played a vital role in the neovascularization of this model. There was no obvious difference among the G, G/T and G/T/GO hydrogels regarding vessel stimulation. Interestingly, the number of blood vessels induced by G/T/GO/Cu hydrogel scaffolds observed at 2 weeks was greater than that at 4 weeks, suggesting that 2 to 3 weeks after implantation may be the optimal period for in vivo neovascularization in our subcutaneous model. In addition, the in vivo biocompatibility and collagen deposition of the implanted hydrogel scaffolds were confirmed by H&E and Masson's trichrome staining (Figure 6c). Consistent with the in vitro results of cytocompatibility, no evident detrimental inflammatory reactions or impaired tissues were found in any of the four groups, and the implanted hydrogels remained relatively integrated and visible 4 weeks after the operation. Similar to the results of this study, a GelMA-based hydrogel (GelMA/PMMA/PDA) placed in cranial defect sites maintained a relatively intact structure at 4 weeks after surgery and gradually degraded from 4 to 8 weeks to make room for newly formed bone tissues.[27] The first 4 weeks of early restoration occupy a critically important position in the whole process of bone repair and remodeling;[58] thus, the implanted G/T/GO/Cu hydrogels with good structure, during this process, are able to support the defects and result in accelerated formation of new bone tissues.

The most common healing process of bone fractures or defects includes several overlapping stages: inflammatory responses, tissue repair and bone remodeling.[59] Based on the early neovascularization and morphological stability of the G/T/GO/Cu hydrogel scaffolds, achieving collagen deposition and initial new bone tissues is anticipated, making it possible to realize subsequent intramembranous ossification, bone mineralization and bone remodeling in the rat calvarial bone defect model. Moreover, immunofluorescent CD31, F4/80 and CD3 staining were used to determine the neovascularization and macrophage and lymphocyte infiltration of the extracted hydrogel scaffolds, respectively (Figure 6d and e). The density of CD31-positive microvessels randomly obtained from the G/T/GO/Cu hydrogels was obviously higher than that in the other three groups, and the blood vessel density demonstrated a downward trend from 2 to 4 weeks, which corresponded with the visual observation of neovascularization, as shown in Figure 6b. In addition, sparsely distributed CD3-positive T lymphocytes representative of inflammatory infiltration were found in all four groups,[26] especially at 4 w after surgery, confirming the good biocompatibility of the implanted hydrogel scaffolds. In particular, macrophage recruitment or infiltration around the implanted hydrogels was confirmed by immunofluorescent F4/80

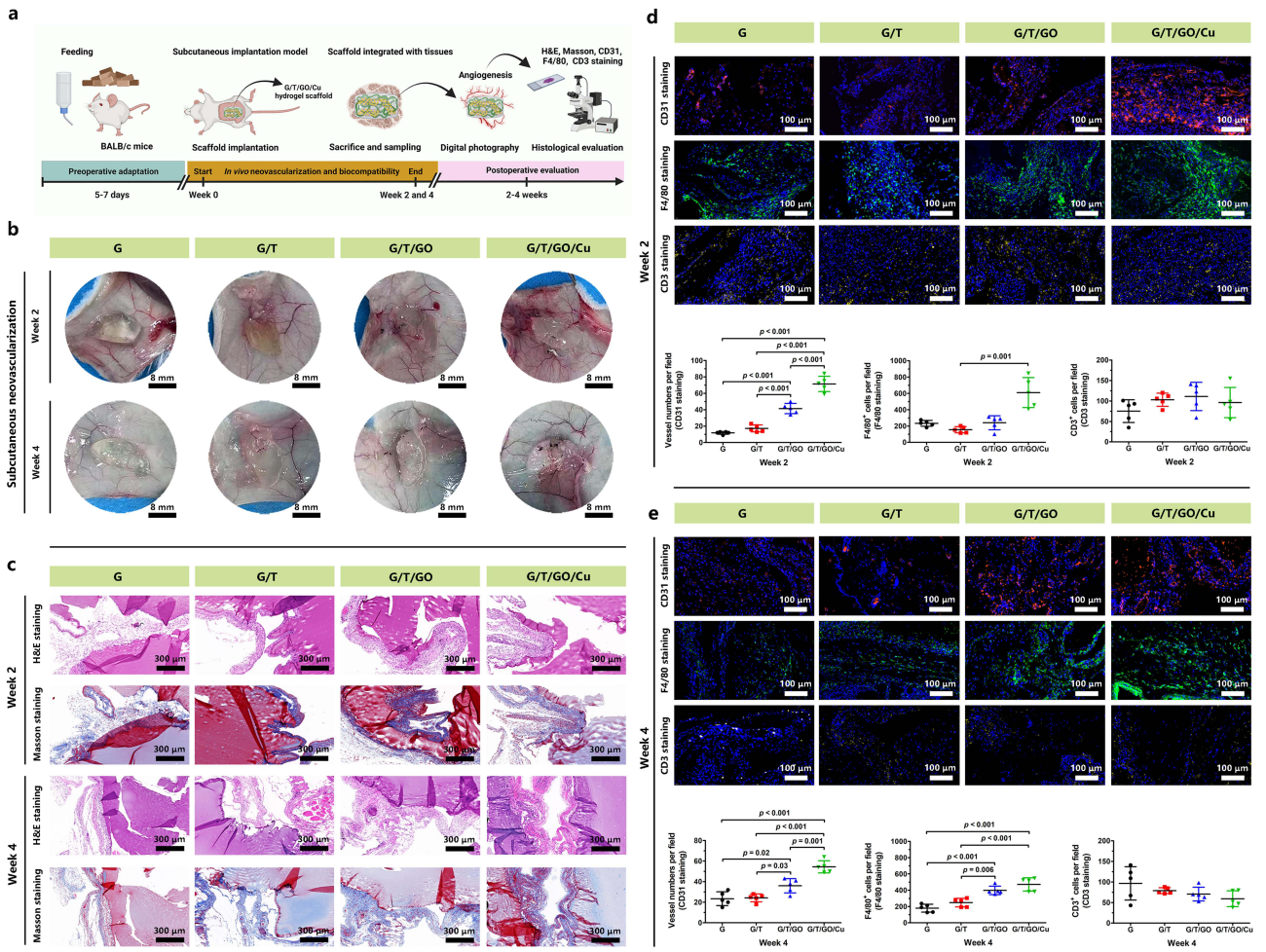

Figure 6 In vivo neovascularization, macrophage recruitment and biocompatibility of the biohybrid hydrogel scaffolds after 2 and 4 weeks of subcutaneous implantation in mice.

Notes: (a) Schematic illustration of the in vivo experimental procedures (created with BioRender. com). **(b)** Representative photographs of neovascularization around the implanted hydrogel scaffolds. **(c)** Histological evaluation of in vivo biocompatibility and collagen deposition of the implanted hydrogel scaffolds as confirmed by H&E and Masson's trichrome staining. **(d, e)** Angiogenesis, macrophage recruitment and lymphocyte infiltration of the extracted hydrogel scaffolds at 2 and 4 weeks as determined by immunofluorescent CD31, F4/80 and CD3 staining, respectively. Quantitative analysis of the corresponding positively stained cells in each randomly selected field (n = 5) was performed and compared.

Abbreviations: CD3, Cluster of Differentiation 3; CD31, Cluster of Differentiation 31; H&E, hematoxylin and eosin.

staining, and significantly greater F4/80-positive macrophages were found in the G/T/GO/Cu hydrogels at the two time points. To further confirm the biological effects of G/T/GO/Cu hydrogels on macrophage polarization, dual immunofluorescent CD206/iNOS staining was conducted as previously reported.[60] CD206 and iNOS are typical markers of M2 and M1 macrophages, respectively. As shown in Figure S6, increased iNOS-positive cells in the harvested samples from the G, G/T and G/T/GO groups at 2 w after implantation indicate a local inflammatory response within the surgical region.[60] In contrast, the G/T/GO/Cu hydrogels induced significantly more CD206 positive cells with an increased ratio of M2/M1 macrophages at 2 w, indicating a promotional effect of copper ions released from the biohybrid hydrogel scaffolds on macrophage M2 polarization in early tissue repair. With the extension of implantation time, all the tested groups exhibited different levels of M2 type polarization at 4 w, especially in the G/T/GO/Cu hydrogels, and the fluorescence intensity of CD206 was also decreased compared to week 2. Our results demonstrated a dynamic process of immune-modulation regulated by the G/T/GO/Cu hydrogels, which was consistent with the in vitro findings as shown in Figure S5, providing a favorable immunomicroenvironment for enhanced bone regeneration in calvarial bone defect model. These findings suggested that the incorporated GO/Cu nanocomposites and release of copper ions could promote macrophage recruitment and M2 type macrophage polarization after injury, especially in the early stage of wound repair.

Macrophage recruitment and polarization have a major effect on inflammatory tissue repair and angiogenesis, and the vascularization of BTE scaffolds mainly depends on the immunomodulatory function of macrophages.[13,61] Moreover, the in vivo biosafety of the biohybrid hydrogel scaffolds was also investigated via histopathological determination of several vital organs (Figure S7). No observed pathological damage was found in the tested sections from the four groups, indicating satisfactory in vivo biosafety of the GO/Cu-incorporated biohybrid hydrogel scaffolds. Considering the direct involvement of macrophages in bone homeostasis, biomaterial-mediated bone repair and bone remodeling,[11] this novel GO/Cu-integrated biohybrid hydrogel scaffold with activated macrophage biology provided new insights into bioengineered scaffold-directed bone regeneration.

In vivo Therapeutic Effects of Biohybrid Hydrogel Scaffolds on the Healing of Calvarial Bone Defects

Based on the systematic evaluation of the in vitro cytocompatibility, macrophage polarization, osteogenic activity and in vivo neovascularization and biocompatibility of the GO/Cu-integrated biohybrid hydrogel scaffolds as previously described and discussed, a rat cranial bone defect model was established to further validate the in vivo bone regeneration potential of the hydrogel scaffolds according to published protocols with some modifications (Figure 7a). [6,31,40] The prepared hydrogels (G/T, G/T/GO and G/T/GO/Cu) were implanted into 4.5 mm full-thickness defects in rat skulls, and cranial defects without hydrogel treatment served as blank controls (Figure S1b). At 6 and 12 weeks after the surgery, 3D reconstruction and 2D images of newly formed bone tissues within the ROIs from the cranial defects were obtained and analyzed using micro-CT scanning. The dynamic and accurate bone healing process after surgery was visualized by consecutive micro-CT images (Figure 7b and c). After 6 weeks of implantation, significantly more newly regenerated and infiltrated bone-like tissues were found around the edge of the cranial defects from the G/T/GO/Cu group compared with those from the other groups. Bone defects with implantation of G/T and G/T/GO hydrogel scaffolds exhibited relatively little bone growth, which means that the addition of β-TCP nanoparticles and GO nanosheets could improve the osteogenic potency of pure GelMA hydrogels. In addition, no obvious new bone formation was observed in the CTRL group, indicating the successful establishment of a critical-sized defect model, as previously confirmed.[4,41,43] After 12 weeks of implantation, the cranial defects filled by G/T/GO/Cu hydrogels were almost covered with newly formed dense bone tissues, whereas the other groups demonstrated obvious defect regions in cranial bone until the end of the animal experiments, especially the CTRL group. Interestingly, the regeneration of new bone tissues initiated from the margins of the defects, moved toward the center and ended at the contralateral sides, which seems inconsistent with the findings of some previous studies.[3,6] Presumably, this discrepancy may be caused by the distribution homogeneity of loaded β-TCP nanoparticles and GO-based nanocomposites within the hydrogel scaffolds, and the in vivo release behavior of copper ions from the hydrogels also had an effect on the recruitment, migration and differentiation of mesenchymal stem cells after surgery, leading to disparate processes of bone mineralization and maturation in the defects. Although bone substitutes prepared with different synthetic technologies have diverse healing profiles during the bone repair process, the ultimate purpose of the implanted BTE scaffolds is to achieve satisfactory recovery with high-quality new bone tissues. In addition, as shown in the 2D images intercepted from the sagittal view, the thickness of the regenerated bone tissues in the G/T/GO/Cu group was also significantly greater than those of the other three groups. Consistent with the 3D reconstructed images, the quantitative analysis of the micro-CT reconstructions indicated that the BV/TV and BS/TV, representative of the degree of bone regeneration obtained from the G/T/GO/Cu, were significantly greater than those of the CTRL group both at 6 and 12 weeks after surgery. Similarly, the values of these bone morphometric data recorded in the G/T/GO group were also higher than those of the CTRL group (Figure 7d). Overall, limited bone regeneration was found in the blank controls, whereas obviously more newly regenerated bone tissues were found in the G/T/GO/Cu group, and the degree of bone regeneration at the two time points displayed a descending trend in the four groups as follows: G/T/GO/Cu > G/T/GO > G/T > CTRL. These results suggested that new bone integration within the defects implanted by the GO/Cu-functionalized hydrogel scaffolds was significantly faster and better than that of the other three groups. In this study, β-TCP, known as one of the most widely used synthetic bone graft substitutes for effective bone regeneration, was incorporated into the hydrogel scaffolds to maintain indispensable osteoinductive, osteoconductive and cell-mediated resorptive properties.[62] The bone repair effect of the G/T and G/T/GO groups observed at 12 weeks was slightly better than that of the blank controls due to the osteogenic potential of β-TCP and GO;[10,22,23,62] however, the biological behaviors of β-TCP or GO were inconsistent under

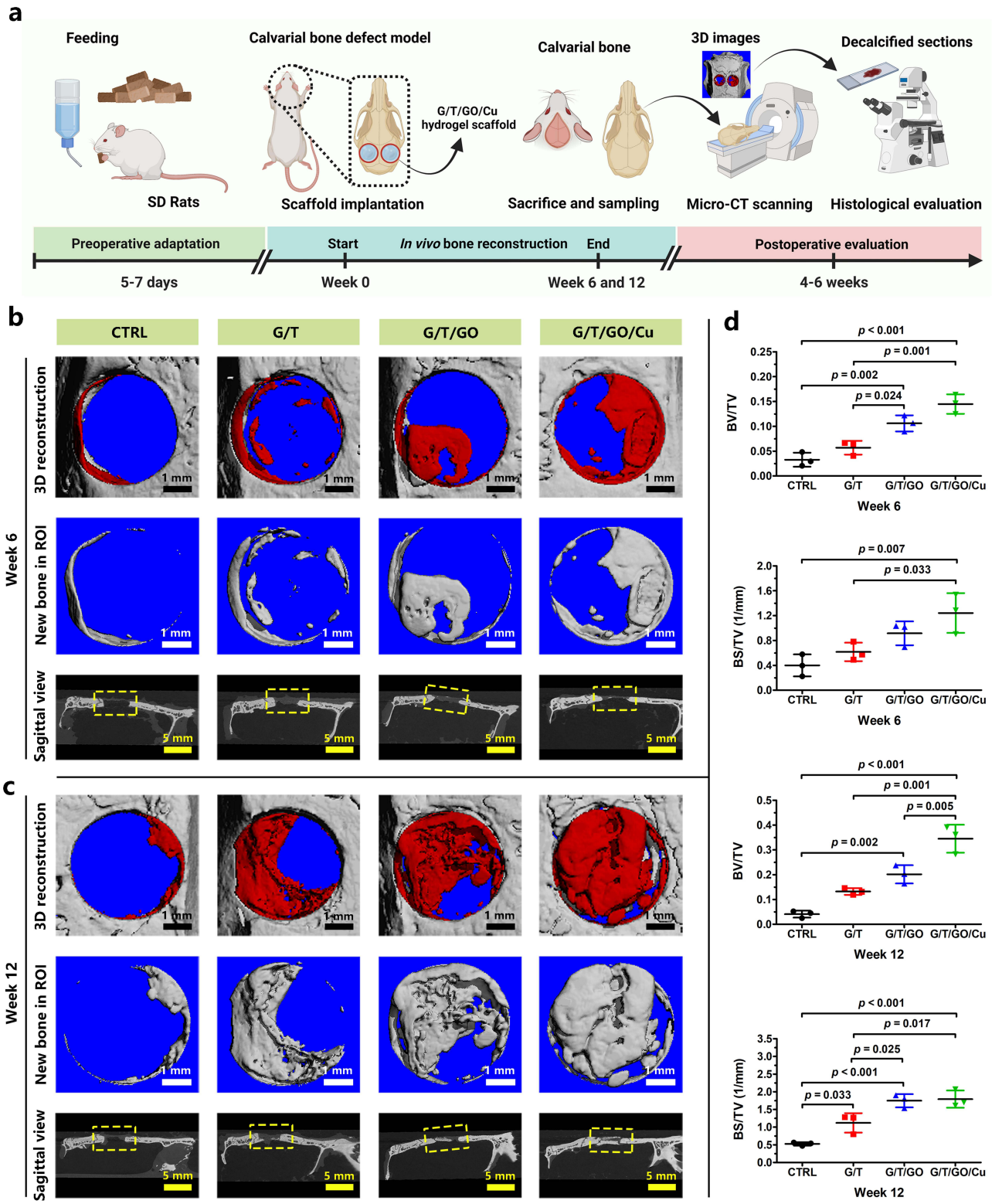

Figure 7 Enhanced bone regeneration induced by GO/Cu-integrated GelMA/TCP hydrogel scaffolds of calvarial bone defects in rats.

Notes: (a) Schematic illustration of the in vivo experimental procedures (created with BioRender. com). **(b)** 3D reconstructed micro-CT images of the calvarial defects at 6 weeks and **(c)** 12 weeks postoperatively. **(d)** Quantitative analysis of relevant bone morphometric data (BV/TV and BS/TV) in selected ROIs of harvested calvarial bone samples at weeks 6 and 12.

Abbreviations: BS/TV, bone surface/total volume; BV/TV, bone volume/total volume; GelMA, methacrylated gelatin; GO/Cu, copper nanoparticle-decorated graphene oxide nanosheets; micro-CT, micro-computerized tomography; ROIs, region of interests; TCP, tricalcium phosphate.

different conditions, which has a direct bearing on the in vivo response of osteogenic cells to the bone graft substitutes.[62,63] To further improve the stability and efficiency of the bioactive materials used for constructing BTE scaffolds, in the present study, the biohybrid hydrogel scaffold effectively, combined with GO/Cu nanocomposites, exhibited evidently promoted osteogenesis functionality that was expected to accelerate bone restoration in a rat calvarial bone defect model.

Subsequently, the in vivo osteogenic potency of the GO/Cu-integrated biohybrid hydrogels was further confirmed, and the detailed morphology of new bone formation within the defect sites was recorded via a series of histological analyses.[41,43,44] As shown in Figure 8, H&E and Masson's trichrome staining were conducted to evaluate the bone healing process of different groups from 6 to 12 weeks. Consistent with the findings of micro-CT reconstructions, significantly less newly formed bone tissues were found in the blank control group without scaffold implantation than those in the other three groups treated with hydrogels at 6 and 12 weeks, suggesting the important role of bone substitutes as bridge connections in accelerating the renovation of critical-size bone defects. It is clear that the CTRL group only had scattered new bone that was mainly composed of fibrous tissues. Particularly, bone defects treated with G/T/GO/Cu exhibited a greater amount of newly formed bone tissues around the degradable hydrogels than that of the G/T and G/T/GO hydrogels, and the cranial defects were almost confluent and filled with well-mineralized bone in the G/T/GO/Cu at 12 weeks after surgery, indicating the excellent bone repair efficacy of the G/T/GO/Cu hydrogel scaffolds in our animal model. Although there were no significant differences between the G/T and G/T/GO groups regarding new bone formation at the two time points after microCT analysis, substitutes with only GO nanosheets still triggered more new bone tissues compared with the G/T group after histological observation. The in vitro results found no significant differences between the G/T and G/T/GO hydrogels in terms of the in vitro enzyme activity of ALP and formation of calcified nodules (Figure 5). The synergistic enhancement of osteogenesis by GO nanosheets and copper nanoparticles was confirmed in our previous study,[25] and bone substitutes incorporated with only GO nanosheets also displayed augmented osteogenic capability via enhancement of BMP-SMAD1/5 signaling pathway.[64] These discrepancies in the in vitro and in vivo osteogenic performances of GO nanosheets may be closely related to the material properties, constitutions, degradable behaviors and biological experimental procedures, which deserves in-depth investigation and elaboration in our future work. Overall, there was no obvious inflammation or necrosis within the bone defects after scaffold implantation, indicating that all the implanted hydrogel scaffolds have good biocompatibility. Similarly, the in vivo biosafety of the biohybrid hydrogel scaffolds in this calvarial bone defect model was also confirmed after H&E staining of the section from the vital organs, which displayed unnoticeable pathological changes after 12 weeks of surgery (Figure S8). Therefore, this GO/Cu-incorporated biohybrid hydrogel scaffold demonstrated stable and acceptable in vivo biosafety and biocompatibility regardless of short- or long-term observation.

To further elucidate the biological effects of implanted GO/Cu-integrated biohybrid hydrogels on in vivo angiogenesis and osteogenesis during the healing of bone defects, immunofluorescence was conducted on corresponding specific protein markers and quantitatively compared based on previously reported protocols (Figure 9).[43,44,65,66] As a typical marker of vascular endothelial cells, CD31 is widely used to evaluate the angiogenic effects of implanted biomaterials, and the expression level of CD31 is highly associated with neovascularization and osteogenesis during bone regeneration.[4,10,43] In this study, significantly greater and denser CD31-positive cells labeled with red fluorescence were observed in the bone slices from the G/T/GO/Cu group when compared with those from the other three groups at weeks 6 and 12, signifying promoted neovascular formation and infiltration induced by the local release of bioactive copper ions from the GO/Cu-decorated composite hydrogels, which further facilitated vascularized osteogenesis and bone regeneration.[37] Meanwhile, more CD31-positive new blood microvessels were found in the G/T/GO group than in the CTRL and G/T groups, which means that the addition of GO nanosheets favored neovascularization and subsequent osteogenesis. Graphene-based biomaterials (GO or rGO) showed synergistically enhanced angiogenesis and osteogenesis, and the angiogenic activities of these two-dimensional materials may be caused by the intracellular formation of reactive oxygen species (ROS) and reactive nitrogen species (RNS) from the local hypoxic microenvironment induced by appropriate doses of GO or rGO.[67] Interestingly, the distribution of CD31-positive cells within the newly formed bone tissues was different at the early and later stages of bone repair, and positively stained cells were mainly located in newly regenerated periosteum and bone tissues at 6 and 12 weeks, respectively, which reflects the dynamic healing process of bone defects and the close relationship between angiogenesis and osteogenesis. Moreover, two important osteoblast

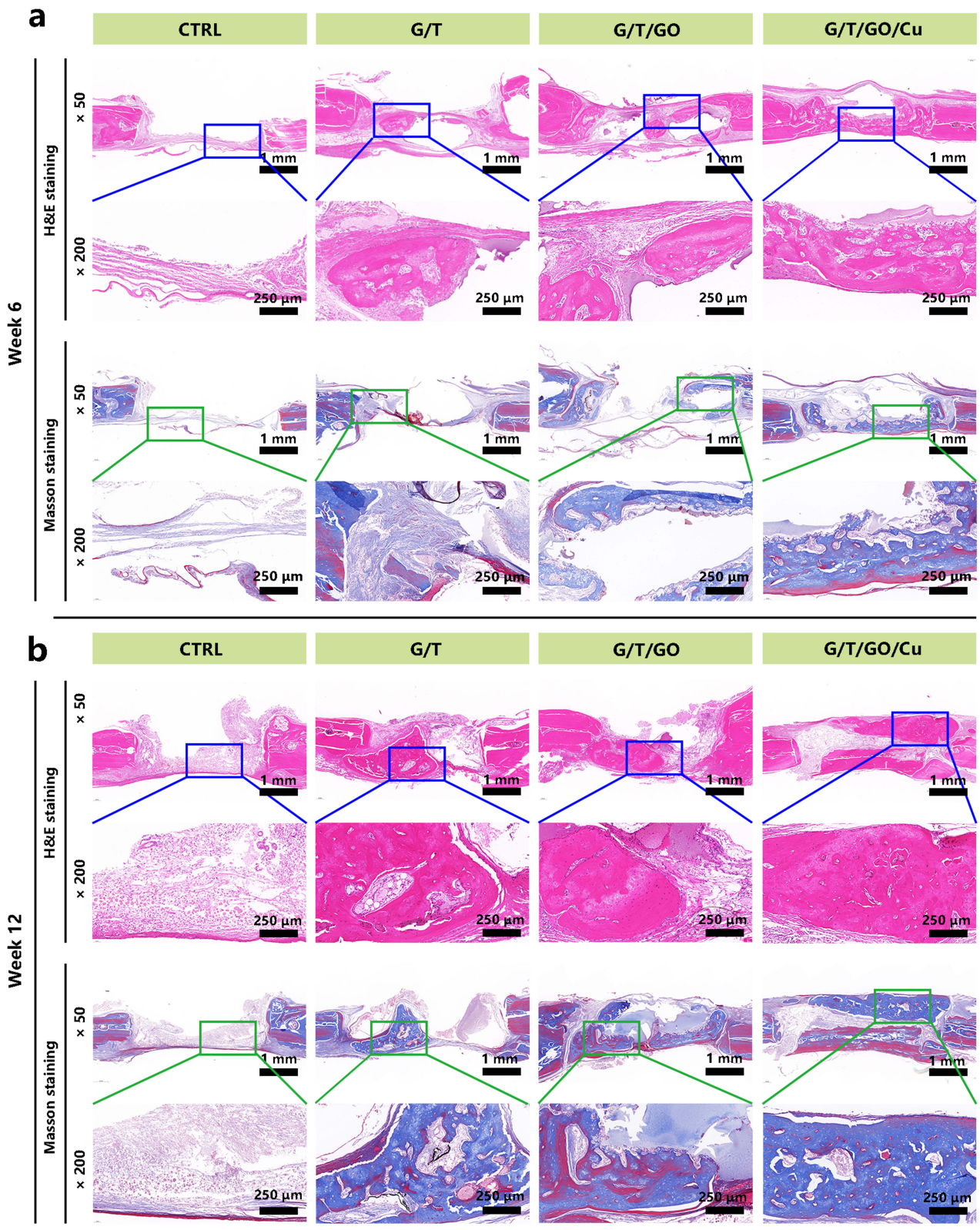

Figure 8 Histomorphological analysis of newly formed bone tissues within calvarial defect areas induced by GO/Cu-integrated GelMA/TCP hydrogel scaffolds.
Notes: (a) H&E and Masson staining of skull specimens harvested from rats at 6 weeks after surgery. **(b)** H&E and Masson staining of skull specimens harvested from rats at 12 weeks after surgery.
Abbreviations: GelMA, methacrylated gelatin; GO/Cu, copper nanoparticle-decorated graphene oxide nanosheets; H&E, hematoxylin and eosin; TCP, tricalcium phosphate.

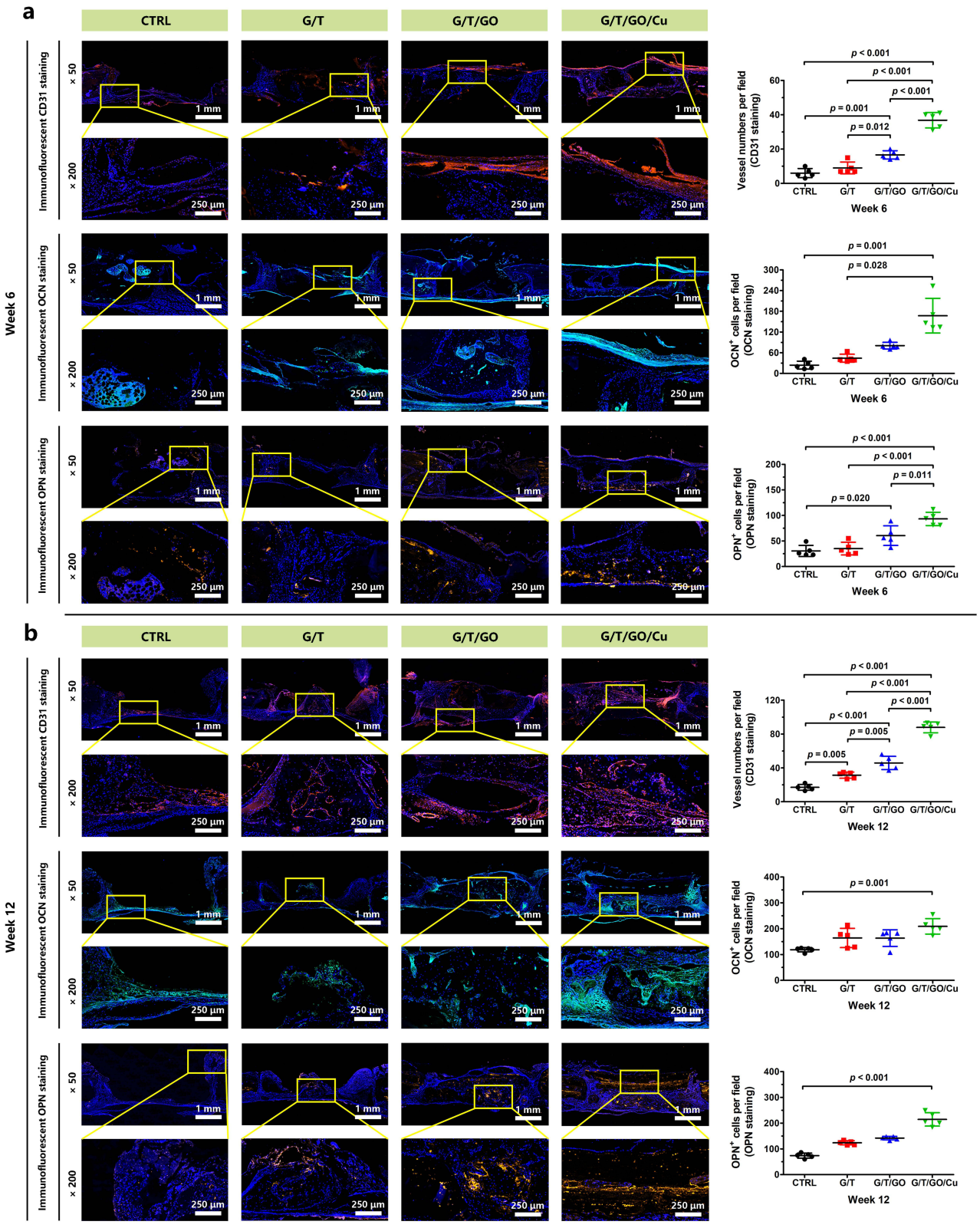

Figure 9 Histomorphological analysis of angiogenesis and bone regeneration-associated specific proteins within the defect areas induced by GO/Cu-integrated GelMA/TCP hydrogel scaffolds.

Notes: (a) Immunofluorescent CD31, OCN and OPN staining of skull specimens harvested from rats at 6 weeks after surgery. **(b)** Immunofluorescent CD31, OCN and OPN staining of skull specimens harvested from rats at 12 weeks after surgery. Quantitative analysis of the corresponding positively stained cells in each randomly selected field (n = 5) was performed and compared.

Abbreviations: CD31, Cluster of Differentiation 31; GelMA, methacrylated gelatin; GO/Cu, copper nanoparticle-decorated graphene oxide nanosheets; TCP, tricalcium phosphate; OCN, osteocalcin; OPN, osteopontin.

markers, OCN and OPN, were also utilized to assess the osteogenic capabilities of the bioactive hydrogel scaffolds.[44,65] Accordingly, bone defects implanted with GO/Cu-modified hydrogels displayed more OCN- or OPN-positive expression areas compared with those of the other three groups at both 6 and 12 weeks, which was in agreement with the in vitro osteogenesis results (Figure 5). These findings provide direct evidence that the GO/Cu-integrated biohybrid hydrogels can effectively accelerate bone growth by stimulating angiogenesis and osteogenesis. More importantly, long-term observation and investigation of material degradation, bone repair efficacy, biocompatibility and biosafety are highly recommended prior to the widespread clinical application.

Conclusion

In the present study, an effective and accessible therapeutic platform, based on biocompatible inorganic substances and degradable hydrogels for synergistic enhancement of osteogenesis, was prepared by integrating GO/Cu nanocomposites into β-TCP/GelMA biohybrid scaffolds via a photocrosslinking technique. The GO/Cu-modified hydrogel scaffolds with sponge-like structures showed good swelling, rheological and biodegradable properties, followed by controlled release behavior of copper ions at different pH values. These biohybrid hydrogel scaffolds exhibited good cytocompatibility with rBMSCs, promoted M2 type macrophage polarization and increased secretion of anti-inflammatory factors, and the incorporation of GO/Cu nanocomposites into the organic-inorganic matrix serving as a bone substitute displayed remarkably promoted osteogenic capability. Then, a subcutaneous implantation model in mice confirmed the in vivo neovascularization, biocompatibility and macrophage biological activation of GO/Cu-functionalized hydrogel scaffolds. Subsequently, a rat cranial bone defect model was established to further validate the in vivo bone regeneration potential of the hydrogel scaffolds, which demonstrated effectively accelerated bone regeneration with stimulated in vivo angiogenesis and osteogenesis. Based on these results, this easily accessible GO/Cu-functionalized biohybrid hydrogel scaffold with biomimetic microstructure, excellent osteopromotive potency, improved inflammatory microenvironment and good biosafety offers an alternative strategy for the effective repair of cranial or mandibular defects in future plastic surgery.

Acknowledgments

This work was supported by the National Natural Science Foundation of China (Nos. 82272293 and 81802136), the Natural Science Foundation of Hunan Province (Nos. 2023JJ30962 and 2020JJ5939), the National Natural Science Foundation of China (Nos. 81974297, 81171813 and 30772254), the Natural Science Foundation of Hunan Province (Nos. 2020JJ4907), the Postdoctoral Science Foundation of China (Nos. 2018M643005) and the Science Foundation for Youth of Xiangya Hospital, Central South University (Nos. 2017Q18). In addition, we want to acknowledge Shiyanjia Lab (www.shiyanjia.com) for providing assistance to the materials characterizations in this work. In addition, this paper has been uploaded to Research Square as a preprint: https://www.researchgate.net/publication/374014735_Graphene_oxidecopper_nanosheet_integrated_hydrogel_platform_as_a_bioactive_and_biocompatible_scaffold_to_accelerate_-calvarial_defect_restoration-preprint.

Disclosure

The authors report no conflicts of interest in this work.

References

1. MacIsaac ZM, Henderson SE, Shakir S, et al. Biomechanical integrity in craniofacial surgery: calvarial reconstruction in favorable and infected defects with bone morphogenetic protein 2. *Plast Reconstr Surg*. 2017;139(5):1141–1150. doi:10.1097/PRS.0000000000003261
2. Kim YC, Yoon IA, Woo SH, et al. Complications arising from clinical application of composite polycaprolactone/bioactive glass ceramic implants for craniofacial reconstruction: a prospective study. *J Craniomaxillofac Surg*. 2022;50(12):863–872. doi:10.1016/j.jcms.2023.01.003
3. Miao Y, Chen Y, Luo J, et al. Black phosphorus nanosheets-enabled DNA hydrogel integrating 3D-printed scaffold for promoting vascularized bone regeneration. *Bioact Mater*. 2022;21:97–109. doi:10.1016/j.bioactmat.2022.08.005
4. Xu Y, Xu C, He L, et al. Stratified-structural hydrogel incorporated with magnesium-ion-modified black phosphorus nanosheets for promoting neuro-vascularized bone regeneration. *Bioact Mater*. 2022;16:271–284. doi:10.1016/j.bioactmat.2022.02.024
5. Ho-Shui-Ling A, Bolander J, Rustom LE, Johnson AW, Luyten FP, Picart C. Bone regeneration strategies: engineered scaffolds, bioactive molecules and stem cells current stage and future perspectives. *Biomaterials*. 2018;180:143–162. doi:10.1016/j.biomaterials.2018.07.017

6. Zhou C, Luo C, Liu S, et al. Pearl-inspired graphene oxide-collagen microgel with multi-layer mineralization through microarray chips for bone defect repair. *Mater Today Bio*. 2022;15:100307. doi:10.1016/j.mtbio.2022.100307
7. Fang X, Xie J, Zhong L, et al. Biomimetic gelatin methacrylamide hydrogel scaffolds for bone tissue engineering. *J Mater Chem B*. 2016;4 (6):1070–1080. doi:10.1039/C5TB02251G
8. Koushik TM, Miller CM, Antunes E. Bone tissue engineering scaffolds: function of multi-material hierarchically structured scaffolds. *Adv Healthc Mater*. 2023;12(9):e2202766. doi:10.1002/adhm.202202766
9. Zhou J, Zhang Z, Joseph J, et al. Biomaterials and nanomedicine for bone regeneration: progress and future prospects. *Exploration*. 2021;1 (2):20210011. doi:10.1002/EXP.20210011
10. Han X, Sun M, Chen B, et al. Lotus seedpod-inspired internal vascularized 3D printed scaffold for bone tissue repair. *Bioact Mater*. 2020;6 (6):1639–1652. doi:10.1016/j.bioactmat.2020.11.019
11. Kim YH, Oreffo ROC, Dawson JI. From hurdle to springboard: the macrophage as target in biomaterial-based bone regeneration strategies. *Bone*. 2022;159:116389. doi:10.1016/j.bone.2022.116389
12. Sun X, Ma Z, Zhao X, et al. Three-dimensional bioprinting of multicell-laden scaffolds containing bone morphogenic protein-4 for promoting M2 macrophage polarization and accelerating bone defect repair in diabetes mellitus. *Bioact Mater*. 2020;6(3):757–769. doi:10.1016/j.bioactmat.2020.08.030
13. Li T, Peng M, Yang Z, et al. 3D-printed IFN-γ-loading calcium silicate-β-tricalcium phosphate scaffold sequentially activates M1 and M2 polarization of macrophages to promote vascularization of tissue engineering bone. *Acta Biomater*. 2018;71:96–107. doi:10.1016/j.actbio.2018.03.012
14. Yue K, Trujillo-de Santiago G, Alvarez MM, Tamayol A, Annabi N, Khademhosseini A. Synthesis, properties, and biomedical applications of gelatin methacryloyl (GelMA) hydrogels. *Biomaterials*. 2015;73:254–271. doi:10.1016/j.biomaterials.2015.08.045
15. Kurian AG, Singh RK, Patel KD, Lee JH, Kim HW. Multifunctional GelMA platforms with nanomaterials for advanced tissue therapeutics. *Bioact Mater*. 2021;8:267–295. doi:10.1016/j.bioactmat.2021.06.027
16. Qiao Y, Liu X, Zhou X, et al. Gelatin templated polypeptide co-cross-linked hydrogel for bone regeneration. *Adv Healthc Mater*. 2020;9(1): e1901239. doi:10.1002/adhm.201901239
17. Tan X, Wu J, Wang R, et al. PgC3Mg metal-organic cages functionalized hydrogels with enhanced bioactive and ROS scavenging capabilities for accelerated bone regeneration. *J Mater Chem B*. 2022;10(28):5375–5387. doi:10.1039/D2TB00907B
18. Liu W, Bi W, Sun Y, et al. Biomimetic organic-inorganic hybrid hydrogel electrospinning periosteum for accelerating bone regeneration. *Mater Sci Eng C Mater Biol Appl*. 2020;110:110670. doi:10.1016/j.msec.2020.110670
19. Zhou B, Jiang X, Zhou X, et al. GelMA-based bioactive hydrogel scaffolds with multiple bone defect repair functions: therapeutic strategies and recent advances. *Biomater Res*. 2023;27(1):86. doi:10.1186/s40824-023-00422-6
20. Yadav S, Singh Raman AP, Meena H, et al. An update on graphene oxide: applications and toxicity. *ACS Omega*. 2022;7(40):35387–35445. doi:10.1021/acsomega.2c03171
21. Jin Y, Zhou J, Zhao X, Zhang X, Su Z. When 2D nanomaterials meet biomolecules: design strategies and hybrid nanostructures for bone tissue engineering. *J Mater Chem B*. 2022;10(44):9040–9053. doi:10.1039/D2TB01489K
22. Du Z, Wang C, Zhang R, Wang X, Li X. Applications of graphene and its derivatives in bone repair: advantages for promoting bone formation and providing real-time detection, challenges and future prospects. *Int J Nanomed*. 2020;15:7523–7551. doi:10.2147/IJN.S271917
23. Zhihui K, Min D. Application of graphene oxide-based hydrogels in bone tissue engineering. *ACS Biomater Sci Eng*. 2022;8(7):2849–2857. doi:10.1021/acsbiomaterials.2c00396
24. Li S, Cui Y, Liu H, et al. Application of bioactive metal ions in the treatment of bone defects. *J Mater Chem B*. 2022;10(45):9369–9388. doi:10.1039/D2TB01684B
25. Yang Y, Li M, Luo H, Zhang D. Surface-decorated graphene oxide sheets with copper nanoderivatives for bone regeneration: an *in vitro* and *in vivo* study regarding molecular mechanisms, osteogenesis, and anti-infection potential. *ACS Infect Dis*. 2022;8(3):499–515. doi:10.1021/acsinfecdis.1c00496
26. Yang Y, Dong Z, Li M, et al. Graphene oxide/copper nanoderivatives-modified chitosan/hyaluronic acid dressings for facilitating wound healing in infected full-thickness skin defects. *Int J Nanomed*. 2020;15:8231–8247. doi:10.2147/IJN.S278631
27. Wu Z, Bai J, Ge G, et al. Regulating macrophage polarization in high glucose microenvironment using lithium-modified bioglass-hydrogel for diabetic bone regeneration. *Adv Healthc Mater*. 2022;11(13):e2200298. doi:10.1002/adhm.202200298
28. Xu Y, Xu C, Yang K, et al. Copper ion-modified germanium phosphorus nanosheets integrated with an electroactive and biodegradable hydrogel for neuro-vascularized bone regeneration. *Adv Healthc Mater*. 2023;12(27):e2301151. doi:10.1002/adhm.202301151
29. Yang F, Xue Y, Wang F, et al. Sustained release of magnesium and zinc ions synergistically accelerates wound healing. *Bioact Mater*. 2023;26:88–101. doi:10.1016/j.bioactmat.2023.02.019
30. Yang Y, Li M, Zhou B, Jiang X, Zhang D, Luo H. Graphene oxide/gallium nanoderivative as a multifunctional modulator of osteoblastogenesis and osteoclastogenesis for the synergistic therapy of implant-related bone infection. *Bioact Mater*. 2023;25:594–614. doi:10.1016/j.bioactmat.2022.07.015
31. Wu Y, Zhang X, Tan B, Shan Y, Zhao X, Liao J. Near-infrared light control of GelMA/PMMA/PDA hydrogel with mild photothermal therapy for skull regeneration. *Biomater Adv*. 2022;133:112641. doi:10.1016/j.msec.2022.112641
32. Yang Y, Liu L, Luo H, Zhang D, Lei S, Zhou K. Dual-purpose magnesium-incorporated titanium nanotubes for combating bacterial infection and ameliorating osteolysis to realize better osseointegration. *ACS Biomater Sci Eng*. 2019;5(10):5368–5383. doi:10.1021/acsbiomaterials.9b00938
33. Zhao H, Xu J, Feng C, et al. Tailoring aggregation extent of photosensitizers to boost phototherapy potency for eliciting systemic antitumor immunity. *Adv Mater*. 2022;34(8):e2106390. doi:10.1002/adma.202106390
34. Shi C, Yu Y, Wu H, et al. A graphene oxide-loaded processed pyritum composite hydrogel for accelerated bone regeneration via mediation of M2 macrophage polarization. *Mater Today Bio*. 2023;22:100753. doi:10.1016/j.mtbio.2023.100753
35. Gu Y, Zhang J, Zhang X, Liang G, Xu T, Niu W. Three-dimensional printed Mg-doped β-TCP bone tissue engineering scaffolds: effects of magnesium ion concentration on osteogenesis and angiogenesis *in vitro*. *Tissue Eng Regen Med*. 2019;16(4):415–429. doi:10.1007/s13770-019-00192-0
36. Zhou X, Wang H, Zhang J, et al. Functional poly(ε-caprolactone)/chitosan dressings with nitric oxide-releasing property improve wound healing. *Acta Biomater*. 2017;54:128–137. doi:10.1016/j.actbio.2017.03.011

37. Yang Y, Xu T, Bei HP, et al. Gaussian curvature-driven direction of cell fate toward osteogenesis with triply periodic minimal surface scaffolds. *Proc Natl Acad Sci U S A*. 2022;119(41):e2206684119. doi:10.1073/pnas.2206684119
38. Nikam SP, Hsu YH, Marks JR, et al. Anti-adhesive bioresorbable elastomer-coated composite hernia mesh that reduce intraperitoneal adhesions. *Biomaterials*. 2023;292:121940. doi:10.1016/j.biomaterials.2022.121940
39. Yuan X, Xiao H, Hu Q, Shen G, Qin X. RGMa promotes dedifferentiation of vascular smooth muscle cells into a macrophage-like phenotype *in vivo* and *in vitro* [published correction appears in J Lipid Res. 2023 Feb;64(2):100331]. *J Lipid Res*. 2022;63(10):100276. doi:10.1016/j.jlr.2022.100276
40. Zhang J, Huang Y, Wang Y, Xu J, Huang T, Luo X. Construction of biomimetic cell-sheet-engineered periosteum with a double cell sheet to repair calvarial defects of rats. *J Orthop Translat*. 2022;38:1–11. doi:10.1016/j.jot.2022.09.005
41. Hu ZC, Lu JQ, Zhang TW, et al. Piezoresistive MXene/Silk fibroin nanocomposite hydrogel for accelerating bone regeneration by re-establishing electrical microenvironment. *Bioact Mater*. 2022;22:1–17. doi:10.1016/j.bioactmat.2022.08.025
42. Yang Y, Chu L, Yang S, et al. Dual-functional 3D-printed composite scaffold for inhibiting bacterial infection and promoting bone regeneration in infected bone defect models. *Acta Biomater*. 2018;79:265–275. doi:10.1016/j.actbio.2018.08.015
43. Xu C, Chang Y, Xu Y, et al. Silicon-phosphorus-nanosheets-integrated 3D-printable hydrogel as a bioactive and biodegradable scaffold for vascularized bone regeneration. *Adv Healthc Mater*. 2022;11(6):e2101911. doi:10.1002/adhm.202101911
44. Li Z, Li S, Yang J, et al. 3D bioprinted gelatin/gellan gum-based scaffold with double-crosslinking network for vascularized bone regeneration. *Carbohydr Polym*. 2022;290:119469. doi:10.1016/j.carbpol.2022.119469
45. Ma W, Soroush A, Luong TVA, Rahaman MS. Cysteamine- and graphene oxide-mediated copper nanoparticle decoration on reverse osmosis membrane for enhanced anti-microbial performance. *J Colloid Interface Sci*. 2017;501:330–340. doi:10.1016/j.jcis.2017.04.069
46. Jo YK, Choi BH, Kim CS, Cha HJ. Diatom-inspired silica nanostructure coatings with controllable microroughness using an engineered mussel protein glue to accelerate bone growth on titanium-based implants. *Adv Mater*. 2017;29(46):1704906. doi:10.1002/adma.201704906
47. Yang Y, Ao H, Wang Y, et al. Cytocompatibility with osteogenic cells and enhanced *in vivo* anti-infection potential of quaternized chitosan-loaded titania nanotubes. *Bone Res*. 2016;4(1):16027. doi:10.1038/boneres.2016.27
48. Hu X, Mei S, Wang F, et al. A microporous surface containing Si3N4/Ta microparticles of PEKK exhibits both antibacterial and osteogenic activity for inducing cellular response and improving osseointegration. *Bioact Mater*. 2021;6(10):3136–3149. doi:10.1016/j.bioactmat.2021.02.027
49. Muzzarelli RA, El Mehtedi M, Bottegoni C, Gigante A. Physical properties imparted by genipin to chitosan for tissue regeneration with human stem cells: a review. *Int J Biol Macromol*. 2016;93(Pt B):1366–1381. doi:10.1016/j.ijbiomac.2016.03.075
50. Abdollahi Baghban S, Ebrahimi M, Bagheri-Khoulenjani S, Khorasani M. A highly efficient microwave-assisted synthesis of an LED-curable methacrylated gelatin for bio applications. *RSC Adv*. 2021;11(25):14996–15009. doi:10.1039/D1RA01269J
51. Fang B, Qiu P, Xia C, et al. Extracellular matrix scaffold crosslinked with vancomycin for multifunctional antibacterial bone infection therapy. *Biomaterials*. 2021;268:120603. doi:10.1016/j.biomaterials.2020.120603
52. Motasadizadeh H, Tavakoli M, Damoogh S, et al. Dual drug delivery system of teicoplanin and phenamil based on pH-sensitive silk fibroin/sodium alginate hydrogel scaffold for treating chronic bone infection. *Biomater Adv*. 2022;139:213032. doi:10.1016/j.bioadv.2022.213032
53. Gupta R, Swarupa S, Mayya C, Bhatia D, Thareja P. Graphene oxide-carbamoylated chitosan hydrogels with tunable mechanical properties for biological applications. *ACS Appl Bio Mater*. 2023;6(2):578–590. doi:10.1021/acsabm.2c00885
54. Liao KH, Lin YS, Macosko CW, Haynes CL. Cytotoxicity of graphene oxide and graphene in human erythrocytes and skin fibroblasts. *ACS Appl Mater Interfaces*. 2011;3(7):2607–2615. doi:10.1021/am200428v
55. Xue Q, Kang R, Klionsky DJ, Tang D, Liu J, Chen X. Copper metabolism in cell death and autophagy. *Autophagy*. 2023;19(8):2175–2195. doi:10.1080/15548627.2023.2200554
56. Sui B, Ding T, Wan X, et al. Piezoelectric stimulation enhances bone regeneration in alveolar bone defects through metabolic reprogramming of macrophages. *Exploration*. 2024. doi:10.1002/EXP.20230149
57. Zhu C, Han S, Zeng X, Zhu C, Pu Y, Sun Y. Multifunctional thermo-sensitive hydrogel for modulating the microenvironment in Osteoarthritis by polarizing macrophages and scavenging RONS. *J Nanobiotechnology*. 2022;20(1):221. doi:10.1186/s12951-022-01422-9
58. Bi F, Chen Y, Liu J, Hu W, Tian K. Bone mesenchymal stem cells contribute to ligament regeneration and graft-bone healing after anterior cruciate ligament reconstruction with silk-collagen scaffold. *Stem Cells Int*. 2021;2021:6697969. doi:10.1155/2021/6697969
59. Sivakumar PM, Yetisgin AA, Sahin SB, Demir E, Cetinel S. Bone tissue engineering: anionic polysaccharides as promising scaffolds. *Carbohydr Polym*. 2022;283:119142. doi:10.1016/j.carbpol.2022.119142
60. Yu X, Jiang S, Li D, et al. Osteoimmunomodulatory bioinks for 3D bioprinting achieve complete regeneration of critical-sized bone defects. *Compos B Eng*. 2024;273:111256. doi:10.1016/j.compositesb.2024.111256
61. Roh JD, Sawh-Martinez R, Brennan MP, et al. Tissue-engineered vascular grafts transform into mature blood vessels via an inflammation-mediated process of vascular remodeling. *Proc Natl Acad Sci U S A*. 2010;107(10):4669–4674. doi:10.1073/pnas.0911465107
62. Bohner M, Santoni BLG, Döbelin N. β-tricalcium phosphate for bone substitution: synthesis and properties. *Acta Biomater*. 2020;113:23–41. doi:10.1016/j.actbio.2020.06.022
63. Peng Z, Zhao T, Zhou Y, Li S, Li J, Leblanc RM. Bone tissue engineering via carbon-based nanomaterials. *Adv Healthc Mater*. 2020;9(5):e1901495. doi:10.1002/adhm.201901495
64. Li Z, Xiang S, Lin Z, et al. Graphene oxide-functionalized nanocomposites promote osteogenesis of human mesenchymal stem cells via enhancement of BMP-SMAD1/5 signaling pathway. *Biomaterials*. 2021;277:121082. doi:10.1016/j.biomaterials.2021.121082
65. Xu C, Xia Y, Zhuang P, et al. FePSe3-nanosheets-integrated cryogenic-3D-printed multifunctional calcium phosphate scaffolds for synergistic therapy of osteosarcoma. *Small*. 2023;19(38):e2303636. doi:10.1002/smll.202303636
66. Ha Y, Ma X, Li S, et al. Bone microenvironment-mimetic scaffolds with hierarchical microstructure for enhanced vascularization and bone regeneration. *Adv Funct Mater*. 2022;32(20):2200011. doi:10.1002/adfm.202200011
67. Mukherjee S, Sriram P, Barui AK, et al. Graphene oxides show angiogenic properties. *Adv Healthc Mater*. 2015;4(11):1722–1732. doi:10.1002/adhm.201500155